AGU PUBLICATIONS

Geochemistry, Geophysics, Geosystems

RESEARCH ARTICLE

10.1002/2017GC007071

Key Points:
- Modern Monterey Canyon incision started between 10 and 7 Ma and was associated with extensive riverine input of terrestrial material
- Southern Sierra Nevada or western Basin and Range are the most likely sources of terrestrial material into the canyon around 7 Ma
- Ferromanganese crusts near the Monterey Canyon show trends toward more radiogenic seawater Os, Nd, and Pb isotopes from ~6.8 to 4.5 Ma

Supporting Information:
- Supporting Information S1
- Data Set S1
- Data Set S2
- Data Set S3
- Data Set S4

Correspondence to:
T. A. Conrad,
tconrad@ucsc.edu

Citation:
Conrad, T. A., Nielsen, S. G., Peucker-Ehrenbrink, B., Blusztajn, J., Winslow, D., Hein, J. R., & Paytan, A. (2017). Reconstructing the evolution of the submarine Monterey Canyon System from Os, Nd, and Pb isotopes in hydrogenetic Fe-Mn crusts. *Geochemistry, Geophysics, Geosystems*, *18*, 3946–3963. https://doi.org/10.1002/2017GC007071

Received 19 JUN 2017
Accepted 10 OCT 2017
Accepted article online 16 OCT 2017
Published online 15 NOV 2017

Reconstructing the Evolution of the Submarine Monterey Canyon System From Os, Nd, and Pb Isotopes in Hydrogenetic Fe-Mn Crusts

T. A. Conrad[1,2], S. G. Nielsen[2], B. Peucker-Ehrenbrink[2], J. Blusztajn[2], D. Winslow[1], J. R. Hein[3], and A. Paytan[4]

[1]University California Santa Cruz, E&PS, Santa Cruz, CA, USA, [2]Woods Hole Oceanographic Institution, Woods Hole, MA, USA, [3]U.S. Geological Survey, PCMSC, Santa Cruz, CA, USA, [4]University California Santa Cruz, Institute of Marine Sciences, Santa Cruz, CA, USA

Abstract The sources of terrestrial material delivered to the California margin over the past 7 Myr were assessed using $^{187}Os/^{188}Os$, Nd, and Pb isotopes in hydrogenetic ferromanganese crusts from three seamounts along the central and southern California margin. From 6.8 to 4.5 (±0.5) Ma, all three isotope systems show more radiogenic values at Davidson Seamount, located near the base of the Monterey Canyon System, than in Fe-Mn crusts from the more remote Taney and Hoss Seamounts. At the Taney Seamounts, approximately 225 km farther offshore from Davidson Seamount, $^{187}Os/^{188}Os$ values, but not Pb and Nd isotope ratios, also deviate from the Cenozoic seawater curve toward more radiogenic values from 6.8 to 4.5 (±0.5) Ma. However, none of the isotope systems in Fe-Mn crusts deviate from seawater at Hoss Seamount located approximately 450 km to the south. The regional gradients in isotope ratios indicate that substantial input of dissolved and particulate terrestrial material into the Monterey Canyon System is responsible for the local deviations in the seawater Nd, Pb, and Os isotope compositions from 6.8 to 4.5 (±0.5) Ma. The isotope ratios recorded in Fe-Mn crusts are consistent with a southern Sierra Nevada or western Basin and Range provenance of the terrestrial material which was delivered by rivers to the canyon. The exhumation of the modern Monterey Canyon must have begun between 10 and 6.8 ± 0.5 Ma, as indicated by our data, the age of incised strata, and paleo-location of the Monterey Canyon relative to the paleo-coastline.

Plain Language Summary The Monterey Submarine Canyon is the main feature of Monterey Bay, California and is as large as the Grand Canyon, but little is known about the age of the Monterey Canyon and how it formed. We used iron and manganese-rich rocks that grew out of seawater (ferromanganese crusts) that formed near the Monterey Canyon and recorded seawater chemistry to study changes in the material transported from land to sea. This information combined with the location of the Monterey Canyon along the California coastline was used to determine that the modern Monterey Canyon started forming between about 10 and 6.8 million years ago. Specifically, we show that the Monterey Canyon is at least 6.8 million years old. The Monterey Canyon was likely carved by a river or rivers carrying large amounts of material from the continent into the ocean and through the canyon. This ended when the mountains of the California Coast Range along Southern California rose up about 5 million years ago.

1. Introduction

The Monterey Canyon (MC) is the main channel of the Monterey Canyon System (MCS) and the dominant feature of central California's Monterey Bay National Marine Sanctuary (Eittreim et al., 2002; Greene & Hicks, 1990; Greene et al., 1989). Comparable to the Grand Canyon, the MC has a maximum vertical relief of 1,700 m, width of ~12 km, and length including the fan-valley of 470 km (Greene et al., 2002). The MCS includes six canyons with 16 canyon heads and extends 153 km off the modern shoreline, reaching a depth of 3,600 m below sea level (Greene & Hicks, 1990; Greene et al., 2002). It has been proposed that the MCS was initially incised in the Oligocene to early Miocene (33.9–15.97 Ma), near the current location of California's Transverse Range, possibly subaerially (Greene, 1977; Greene & Hicks, 1990). That paleo MC was then filled and reexhumed possibly more than once to form the modern MC (Greene, 1977; Greene & Hicks, 1990). Today, the Monterey and Carmel canyons are the only canyons in the Monterey Bay region extending

to the shoreline. Several rivers including the Pajaro River, San Lorenzo River, and Soquel Creek drain into Monterey Bay north of the MC and transport sediment into Monterey Bay, but only the Salinas River and Elkhorn Slough feed into the MC at Moss Landing (Best & Griggs, 1991; Eittreim et al., 2002; Greene et al., 2002). Active sediment deposition during the modern sea level highstand in the MC is also observed in submarine canyons studied off southern California (Covault et al., 2007; Eittreim et al., 2002). In addition to fluvial sediments, the MCS also traps sediment carried by longshore currents and from local erosion of sea cliffs (Best & Griggs, 1991; Eittreim et al., 2002; Greene et al., 2002). Turbidity currents episodically carry trapped sediment down-canyon and cause further canyon incision (Covault et al., 2007; Greene & Hicks, 1990; Paull et al., 2003).

Despite this significant body of work on the MCS and its evolution, the age and initial formation of the modern MC and MCS are poorly known with little direct age information available to pinpoint the onset and duration of canyon incision. Here we use records of paleo-seawater chemistry archived in hydrogenetic ferromanganese (Fe-Mn) crusts collected from seamounts located close to the MC submarine fan to shed new light on the timing and sources of terrestrial inputs into the California margin proximal to the canyon system.

2. Tectonic and Geological Background

The MCS lies along an active tectonic margin spanning the boundary of the Pacific and North American plates (Anima et al., 2002; Eittreim et al., 2002; Greene et al., 2002). The region is dominated by right-lateral strike slip movement along the San Andreas and San Gregorio Fault systems (Anima et al., 2002). The MCS primarily cuts into the allochthonous Salinian block, which is bounded to the east by the San Andreas Fault, to the west by the San Gregorio Fault, and is mainly composed of Cretaceous granite (Anima et al., 2002; Barbeau et al., 2005; Greene, 1977).

The complex tectonic environment makes reconstructing movement difficult. It is thought that parts of the Ascension Canyon system, north of the MC, including the Ascension, Año Nuevo, and Cabrillo canyons (Figure 1), originated as a channel to the MC during the Pliocene lowstand (~3.8 Ma) and have undergone northward migration relative to the MC (Greene & Hicks, 1990; Nagel et al., 1986). Greene and Hicks (1990) proposed that if this is true, then right lateral motion and excavation of the canyon systems may have increased, starting at around 10–7 Ma, based on the increased distances between canyons of the Ascension Canyon System (1–4 km apart, Figure 1, numbers 3–5) and those of the MCS (around 30 km apart, Figure 1, numbers 5–7) (Greene & Hicks, 1990).

Sedimentary particulate and dissolved inputs through the MCS and sediment deposition on the continental shelf and in the Monterey Fan are affected by tectonic, eustatic, climatic, and oceanographic processes (Edwards, 2002; Griggs & Hein, 1980; Lewis et al., 2002). Rivers are the main source of sedimentary and dissolved material to the California margin (Best & Griggs, 1991; Griggs & Hein, 1980). Anthropogenic activities such as mining, agriculture, and timber harvesting tend to increase sediment fluxes whereas reservoir construction and conservation activities decrease sediment fluxes (Griggs & Hein, 1980; Jeandel & Oelkers, 2015; Meade, 1969). Modern river sediment fluxes are therefore of questionable value in establishing volumes and sources of paleo-inputs.

Reconstructing the stratigraphy of sedimentary sequences in the Monterey Bay region is also complicated by unconformities. Previous work around the Monterey Bay has shown that primarily Neogene (23.03–2.59 Ma) strata overlies the Mesozoic (251.0–65.5 Ma) basement complex without the presence of Paleogene (65.5–23.03 Ma) deposits (Greene, 1977; Greene & Hicks, 1990). There are also unconformities bounding sedimentary deposits of late Miocene to Pliocene (11.63–5.33 Ma), and late Pliocene to Holocene ages (3.60 Ma to 11.7 ka) (Greene, 1977). Seismic-reflection data show that the MC and some related canyons incised Mesozoic (251.0–65.5 Ma) basement rock. These incisions are filled with middle Miocene (~15.97 to 11.63 Ma) and younger sediment, implying a pre-middle Miocene (pre 15.97 Ma) origin for the paleo-canyons (Greene, 1977; Greene & Hicks, 1990). Uninterrupted sedimentation occurred in the Monterey Bay region during the middle to late Miocene (15.97–5.33 Ma), as indicated by conformable strata filling canyons in the upper MCS near the coastline on seismic-reflection profiles. The modern MC cuts through this material indicating incision of the canyon occurred since the late-middle Miocene (~11.63 Ma) (Greene, 1977; Greene & Hicks, 1990). Formation of the modern MC is thought to have begun in the late Pliocene (3.60 Ma) by

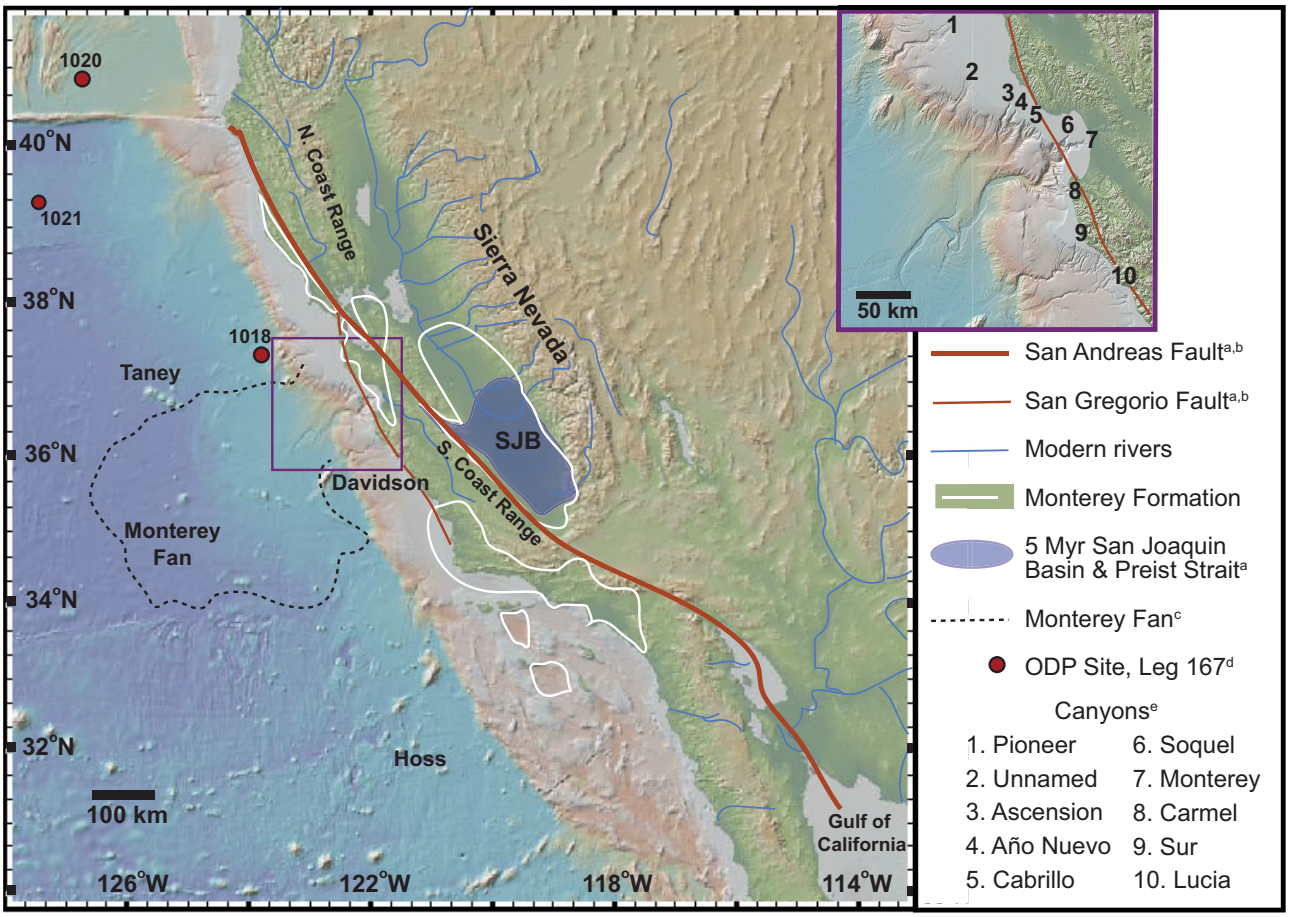

Figure 1. Location map of the central and southern California coast with the Davidson, Taney, and Hoss Seamounts, Ascension-Monterey Submarine Canyon System and Fan, San Andreas Fault, San Gregorio Fault, and Paleo San Joaquin Basin with Priest Strait, indicated (GeomapApp.org; Ryan et al., 2009). References, subscripts in key: a. Bowersox (2005); b. Anima et al. (2002); c. Fildani and Normark (2004); d. Lyle et al. (2000); e. Greene and Hicks (1990).

erosion of canyon fill from seaward sediment transport (Greene & Hicks, 1990). It has also been proposed that the MC was reexhumed during two separate events occurring in the late Miocene (11.63–5.33 Ma) and the Pleistocene (<2.59 Ma) (Greene, 1977; Greene & Hicks, 1990).

The coastline has moved westward toward the modern position since 20 Ma (Bowersox, 2005). From 10 to 5 Ma the coastline was further east (inland) than today (Bowersox, 2005; Müller et al., 2008) (Figure 2). The San Joaquin Basin, southeast of the modern Monterey Bay was connected to the Pacific in the west and extended to the Sierra Nevada Mountains in the east (Johnson & Graham, 2007; Pyenson et al., 2009). By the late Neogene to Pleistocene (5.33 Ma to 11.7 ka), the major rivers draining the southern Sierra Nevada flowed westward, possibly emptying into the San Joaquin Basin (Bowersox, 2004, 2005; Graham et al., 1988; Reid, 1995; Wakabayashi & Sawyer, 2001). This resulted in rates of sediment deposition that equaled or exceeded the rate of basin subsidence, causing gradual progressive shallowing of the basin with a maximum rate of 140 cm/kyr in the early Pliocene (~5.33 Ma) during uplift of the Coast Range (Bowersox, 2004; Loomis, 1990). In the early Pliocene, after the uplift of the Temblor and Gabilan Ranges, in the Southern Coast Range, along the south-western margin of the San Joaquin Basin, the basin was connected to the Pacific only through the Priest Valley Strait, which closed around 2.3 Ma due to tectonic uplift and sedimentation (Bowersox, 2004, 2005; Loomis, 1990).

The inputs into the California margin proximal to the MCS were determined using hydrogenetic Fe-Mn crust records of paleo-seawater chemistry. Ferromanganese crusts grow over millions of years on elevated rock surfaces, such as seamounts, when slope or submarine currents are sufficient to prevent sediment accumulation (Bonatti et al., 1972; Hein & Koschinsky, 2014). Hydrogenetic Fe-Mn crusts commonly grow very slowly

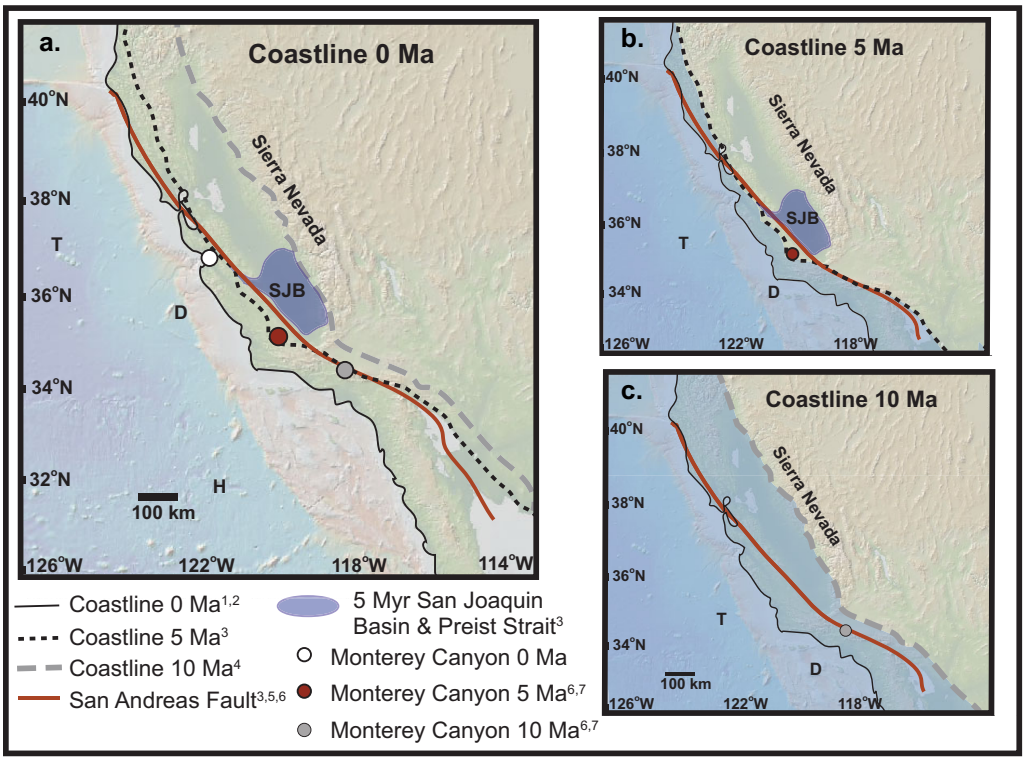

Figure 2. Paleogeographic map of the California margin showing location of the coast line and the Monterey Canyon (MC) at 5 and 10 Ma. (a) The modern coastline with locations of the coastline and MC at present, 5 Ma, and 10 Ma and modern locations of D (Davidson Seamount), T (Taney Seamount Chain), H (Hoss Seamount); (b) the coastline at 5 Ma with estimated paleo-locations for the MC, D, and T; and (c) the coastline at 10 Ma with estimated paleo-locations for the MC, D, and T. The paleo-geographic locations for Davidson Seamount and the Taney Seamount Chain are estimated based on movement of the Pacific Plate. References: 1. GeomapApp.org; 2. Ryan et al. (2009); 3. Bowersox (2005); 4. Müller et al. (2008); 5. Anima et al. (2002); 6. DeMets and Merkouriev (2016); 7. Wilson et al. (2005).

(1–5 mm/Myr) by precipitation of dissolved elements from seawater and they record changes in seawater chemistry over the time of their growth (Halbach & Puteanus, 1984; Hein & Koschinsky, 2014).

Numerous seamounts exist along the California Margin. Hydrogenetic Fe-Mn crust samples were selected from Davidson, Taney B and D, and Hoss Seamounts, which lie on the Pacific Plate (Figure 1). Davidson Seamount is located near the base of the Monterey Submarine Fan (Clague et al., 2009; Davis et al., 2002). Taney B and D Seamounts lie approximately 225 km offshore from the MC. They are part of a chain of five seamounts and formed approximately 26 Ma (Coumans et al., 2015). Hoss Seamount is located significantly farther south of the MCS, offshore of San Diego, and was selected to provide a regional control. Hoss Seamount is estimated to have formed 22–17 Ma (Conrad et al., 2017; Hein et al., 2010).

The geochemical composition of the selected bulk Fe-Mn crust samples has been analyzed previously (Conrad et al., 2017). A hydrogenetic origin was confirmed through the use of trace metal abundance ratios (Bonatti et al., 1972; Conrad et al., 2017). When possible, the thickest crusts from each seamount were chosen, as these are typically the oldest crusts that provide higher temporal resolution and longer duration records. The Fe-Mn crust samples do not show textural evidence of double sided growth, and all except T141-R5 (Davidson) show evidence of attachment to the substrate on the oldest (bottom) surface that would not permit growth from the bottom or overturning of the samples. Consideration was also given to water depth; the two samples from Davidson T145-R9 (3,298 mbsl) and T141-R5 (2,388 mbsl) and the two samples from Taney Seamounts T121-R5 (3,887 mbsl) and D173-R5 (3,178 mbsl) differ in water depth by approximately 1,000 and 700 m, respectively, and may therefore represent different water masses. Hoss Seamount Fe-Mn crust D11-4 was collected from 2,540 to 2,560 mbsl (Conrad et al., 2017).

3. Methods

Ferromanganese crusts were encased in Tap Plastic Clear-Lite Casting Resin and cut using a sintered diamond blade into billets perpendicular to the growth layers (supporting information Text S1). Samples for Os and Nd isotope analyses were subsampled using a New Wave Micromill with Brasslinger 1 mm cylindrical (flat head) diamond tipped drill bit. Osmium was sampled at 2 mm intervals through the crust. Neodymium was sampled at 0.3 mm intervals. However, for both isotope systems not every subsample was analyzed, resulting in a sampling resolution lower than the sampling interval.

All isotope data presented here, $^{187}Os/^{188}Os$, $\varepsilon_{Nd}/^{206}Pb/^{204}Pb$, $^{207}Pb/^{204}Pb$, and $^{208}Pb/^{204}Pb$ were analyzed in the Woods Hole Oceanographic Institution (WHOI) Inductively Coupled Plasma Mass Spectrometer (ICPMS) or Non-traditional Isotope Research on Various Advanced Novel Applications (NIRVANA) facilities using a Thermo Finnigan NEPTUNE multicollector ICP-MS (MC-ICP-MS). Two Fe-Mn crusts were selected from the Hoss, Davidson, and Taney Seamounts (B and D) to measure Os isotopes and create age models. The USGS nodule standard A-1 was digested together with unknown Fe-Mn crust samples using an Anton Parr high-pressure asher (HPA-S).

Osmium isotopes were analyzed with three ion counters using an Ar gas sparging method on the NEPTUNE MC-ICP-MS (Sen & Peucker-Ehrenbrink, 2014). Measurements of Re concentrations on an Element 2 ICP-MS showed that Re concentrations in the Fe-Mn crust samples were extremely low and that in-growth corrections of ^{187}Os to account for the decay of ^{187}Re within the crusts were negligible even in the bottom (oldest) sections of these samples, a finding consistent with previous studies over this time interval (Klemm et al., 2008). The deepest sections of crust measured were D11-4 43–44, T141-R5 31–32, T145-R9 36–37, T121-R5 31–32, and D173-R2 45–46; these samples had Re concentrations (in ng/g) of 0.17, 26.5, 5.94, 1063.5, and 772.8, respectively. Even for T121-R5 with 1,063.5 ng/g Re, the change in the $^{187}Os/^{188}Os$ ratio for that sample resulted in an age difference of less than 0.5 Ma, within the uncertainty of our ability to reconstruct ages. Multiple analysis ($n = 48$) over multiple analytical sessions of the LoOsStd reference standard with an Os concentration of 0.61 pg/g over multiple analytical sessions yielded an average $^{187}Os/^{188}Os$ value of 0.1098 ± 0.0021 (1 standard deviation), within error of the reference value (0.1069 ± 0.0015, $n = 26$) (Sen & Peucker-Ehrenbrink, 2014) (supporting information Text S2, Data Set S1, and Figure S1). Multiple analysis of the USGS A-1 nodule standard, prepared together with the Fe-Mn crust samples, yielded an average $^{187}Os/^{188}Os$ value of 0.969 ± 0.013 ($n = 15$), when three samples with anomalously low $^{187}Os/^{188}Os$ are excluded (supporting information Text S2 and Figure S2). This is the first measurement of $^{187}Os/^{188}Os$ for USGS nodule standard A-1.

Neodymium isotopes were measured in four Fe-Mn crusts, one each from Hoss and Taney B, and two from Davidson Seamounts. Nodule standards USGS A-1 and P-1 were prepared together with the Fe-Mn crust samples. One-stem Nd column chemistry (Scher & Delaney, 2010) utilizing 50–100 μm particle size Eichrom Ln resin to separate and purify Nd, was used, and isotope ratios were analyzed on the MC-ICP-MS following the procedure of Huang et al. (2012). Neodymium isotope ratios for samples and USGS A-1 and P-1 nodule standards are corrected to $^{143}Nd/^{144}Nd = 0.512115$ for JNdi-1 and expressed as ε_{Nd} relative to the Chondritic Uniform Reservoir (CHUR) = 0.512638 (Jacobsen & Wasserburg, 1980; Tanaka et al., 2000). Neodymium was analyzed in the fall of 2014 and the spring of 2015, analyses of the JNdi-1 standard yielded an average $^{143}Nd/^{144}Nd$ of 0.512064 ± 0.000016 (2 standard deviation; $n = 31$), and $^{143}Nd/^{144}Nd = 0.512099 \pm 0.000005$ (2 standard deviation; $n = 14$), respectively, for the two sessions (supporting information Text S3 and Data Set S2). This is compared to the published value for JNdi-1 of 0.512115 ± 0.000007 (Tanaka et al., 2000). Analysis of the USGS A-1 nodule standard ($n = 16$) corrected to JNdi-1 = 0.512115 and averaged over both periods yielded 0.512169 ± 0.000016 ($\varepsilon_{Nd} = -9.15 \pm 0.31$, 2 standard deviation). The published value for nodule A-1 is 0.512148 ± 0.000008 ($\varepsilon_{Nd} = -9.56 \pm 0.16$, 2 standard deviation) (Foster & Vance, 2006a).

Lead isotopes were measured in three Fe-Mn crusts and in pressed pellets of USGS nodule standards A-1 and P-1 using the NewWave/Merchantek NWR-193 ArF excimer laser ablation (LA) system coupled with the NEPTUNE MC-ICP-MS (supporting information Text S4 and Figure S3). A 50 μm diameter laser spot, rastered over a 1 mm line parallel to the growth surface, was used for each subsample, but sampling resolution varied. The ablation cell was purged with He gas. Standard sample bracketing was used to correct for Pb isotope fractionation as the Tl could not be used to correct for mass bias due to low Tl contents in the Fe-Mn crusts as well as potential effects from variations in the stable Tl isotope composition of the crusts (Nielsen

et al., 2009; Rehkämper et al., 2004). To ascertain if instrumental mass bias remained roughly constant throughout the analytical session, we repeatedly analyzed the isotopic difference between the USGS A-1 and P-1 nodule standards (n = 85). For the whole session, we obtained Pb isotope offsets between these two reference materials of $\Delta^{206}Pb/^{204}Pb = 0.253 \pm 0.012$, 1 standard deviation, $\Delta\ ^{207}Pb/^{204}Pb = 0.044 \pm 0.007$, 1 standard deviation, and $\Delta\ ^{208}Pb/^{204}Pb$ 0.248 ± 0.022, 1 standard deviation. These numbers are within error of the published differences of $\Delta^{206}Pb/^{204}Pb = 0.264$, $\Delta\ ^{207}Pb/^{204}Pb = 0.047$, and $\Delta\ ^{208}Pb/^{204}Pb = 0.268$ (Ling et al., 1997). A Python code was written to process the laser ablation Pb isotope data, including background corrections and fractionation corrections based on the paired standards bracketing the samples (supporting information Text S5 and Data Sets S4). A more detailed discussion of the methodology can be found in the supporting information (Foster & Vance, 2006b) (supporting information Figure S4).

4. Results and $^{187}Os/^{188}Os$ Interpretation

4.1. $^{187}Os/^{188}Os$ and Interpreted Ages

Osmium is not subject to significant diffusive re-equilibration in Fe-Mn crusts (Burton et al., 1999; Henderson & Burton, 1999) and has a relatively long residence time in seawater of a few thousand to 50 kyrs (Levasseur et al., 1999). This allows Os to be used to develop age models for the Fe-Mn crust samples by comparing the $^{187}Os/^{188}Os$ of subsamples collected through a crust with the Cenozoic $^{187}Os/^{188}Os$ seawater curve (Burton et al., 1999; Klemm et al., 2005; Nielsen et al., 2009; Peucker-Ehrenbrink & Ravizza, 2012) (see supporting information Text S2, Os isotopes). $^{187}Os/^{188}Os$ was measured in 86 samples from six Fe-Mn crusts and matched with the Cenozoic $^{187}Os/^{188}Os$ seawater curve (supporting information Data Set S1; Figure 3). Ages and growth rates are interpreted from the data that fits on the Cenozoic $^{187}Os/^{188}Os$ seawater curve. Ages and growth rates for sample D11-4 from Hoss Seamount (2,540–2,560 mbsl), the control site, can be adjusted to fit the seawater curve and yield a maximum age of 20.5 ± 0.5 Myr with variable growth rates of 3.6 mm/Myr from 0 to 35 mm, 3.1 mm/Myr from 35 to 39 mm, and 2.2 mm/Myr from 39 to 45mm. Data for Fe-Mn crust samples D173-R2 Taney B, T121-R5 Taney D, and Davidson T145-R9 and T141-R5 fit the seawater curve from approximately 4.5 ± 0.5 Ma to present. Prior to 4.5 ± 0.5 Ma, all four of the Taney and Davidson Seamount Fe-Mn crusts deviate from the Cenozoic seawater Os isotope curve toward more radiogenic values (Figure 3), making direct age determinations by Os isotope stratigraphy impossible for these older sections. Ages for the older sections of these samples were therefore extrapolated using the same

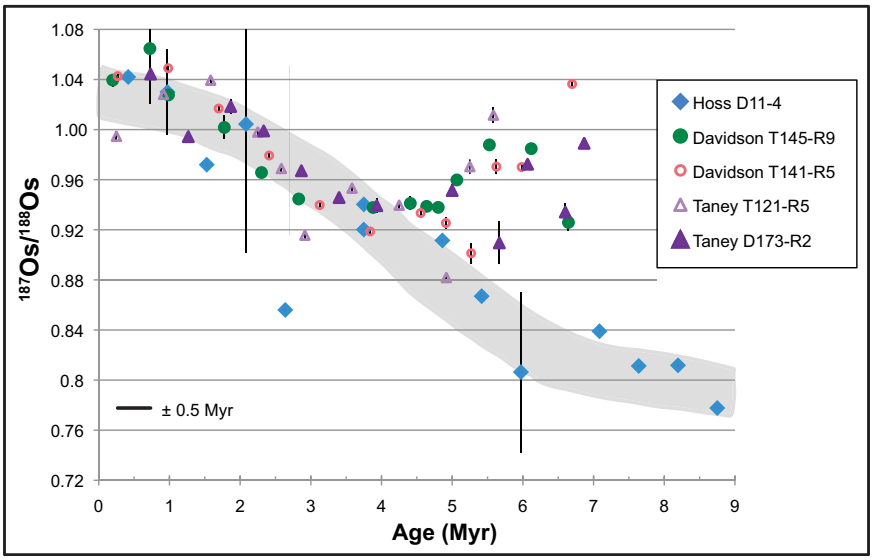

Figure 3. Plot of $^{187}Os/^{188}Os$ in six California margin Fe-Mn crust samples over the past 9 Myr. The gray shaded region represents the Cenozoic $^{187}Os/^{188}Os$ seawater curve (Peucker-Ehrenbrink & Ravizza, 2012). Samples shown in filled symbols were also analyzed for Pb isotopes. Individual Fe-Mn crust samples, including a data point at ~2.7 Ma from Hoss Seamount D11-4, show less radiogenic values relative to the $^{187}Os/^{188}Os$ seawater curve and we attribute these values to the presence of extraterrestrial material.

growth rate as the younger portions, and are also constrained by the age of the substrate on which they grew. Assuming constant growth rates prevents us from detecting rate changes before 4.5 Ma. However, constant growth rates are found to account for all Os isotope variation in crust sections younger than 5.4 Ma, which suggests that the constant growth rate assumption is reasonable for the older sections as well. Extrapolating the growth rates of the younger sections throughout the crusts implies that Fe-Mn crusts T145-R9 and T141-R5 from Davidson Seamount started growing 6.4 ± 0.5 and 6.7 ± 0.5 Ma, respectively, with average growth rates of 7.6 and 5.6 mm/Myr. These maximum ages are younger than the age of Davidson Seamount itself, which has been dated to 14.8–9.8 Ma (Clague et al., 2009). The two crusts from Taney Seamount D and B, T121-R5 and D173-R2 had average growth rates of 6.0 and 7.5 mm/Myr, respectively, which corresponds to ages at the base of the crusts of 5.6 ± 0.5 and 6.8 ± 0.5 Ma, respectively. The deviation to more radiogenic Os isotope values relative to seawater is found at the base of all four crusts from Taney and Davidson Seamounts and, therefore, the process that caused this deviation must predate initiation of Fe-Mn crust growth of the samples studied. Using the extrapolated ages at the base of the Fe-Mn crusts we find that the oldest crust to record the deviation in Os isotopes is D173-R2 from Taney B Seamount with an estimated age of 6.8 ± 0.5 Ma. Thus, the deviation to radiogenic Os isotopes spanned at least 6.8–4.5 Ma, but may have begun earlier.

4.2. Neodymium Isotopes

Neodymium isotopes were measured in 190 samples from four of the six Fe-Mn crusts for which Os isotope age models were created. Ferromanganese crusts D11-4 (Hoss) and D173-R2 (Taney) have ε_{Nd} values consistent with those from central Pacific Fe-Mn crusts (Chen et al., 2013; Frank, 2002; Ling et al., 1997, 2005) (Figure 4; supporting information Data Set S2). Both Davidson Seamount Fe-Mn crusts T145-R9 and T141-R5 deviate in ε_{Nd} toward more radiogenic values around the time when $^{187}Os/^{188}Os$ values deviated from the seawater values. The deviation from regional seawater values, as represented by Hoss D11-4, is particularly prominent in crust T145-R9 as shown in Figure 4 (supporting information Data Set S2). Minor deviations in Hoss D11-4 from the central Pacific Fe-Mn crust reference values are also observed for certain periods in T141-R5, where deviations are slightly greater than the 0.3 ε_{Nd} unit reproducibility of the JNdi-1 standard, and includes four discrete more radiogenic data points (supporting information Data Set S2). The Fe-Mn crust D173-R2 from Taney B Seamount does not show the excursion toward more radiogenic values seen in the older sections of the two Davidson Seamount crusts.

4.3. Lead Isotopes

About 400 samples from three Fe-Mn crusts, D11-4 (188), D173-R2 (87), and T145-R9 (125) from Hoss, Taney, and Davidson Seamounts, respectively, were analyzed for Pb isotopes (supporting information Data Set S3 and Figure S5). The Pb isotope ratios in T145-R9 from Davidson Seamount deviate from regional seawater values as recorded in Hoss Fe-Mn crust D11-4 (Figure 5) in samples older than 5.5 Ma. Two excursions to

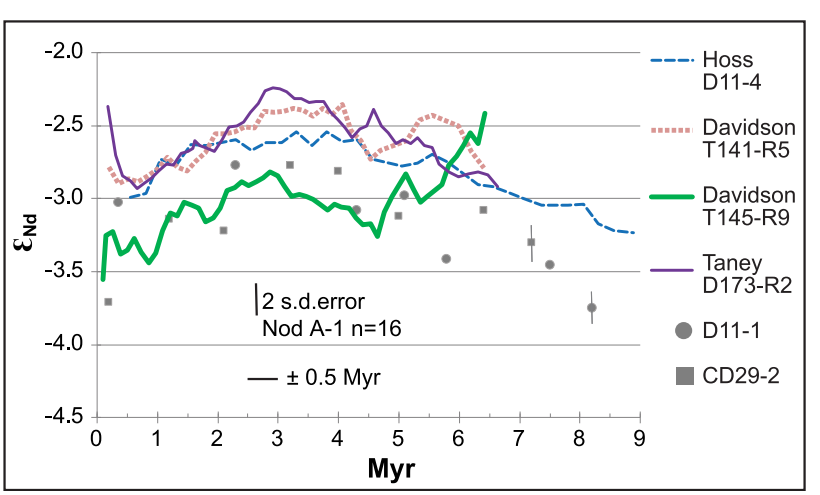

Figure 4. Plot of ε_{Nd} in four California margin Fe-Mn crust samples over the past 9 Myr with data shown as three point moving average trend lines. Central Pacific Fe-Mn crusts D11-1 and CD29-2 are shown for comparison (Ling et al., 1997).

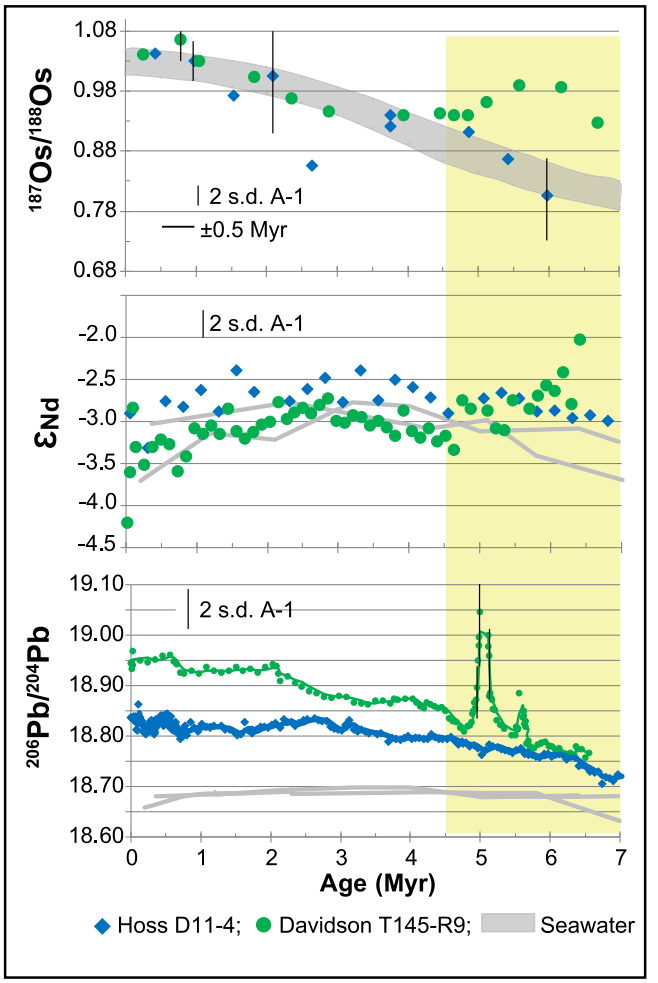

Figure 5. Isotope values for $^{187}Os/^{188}Os$, ε_{Nd}, and $^{206}Pb/^{204}Pb$ for Fe-Mn crust T145-R9, Davidson Seamount are shown relative to Hoss D11-4, representing regional seawater. For ε_{Nd} and $^{206}Pb/^{204}Pb$ Central Pacific seawater, in gray, is represented by Fe-Mn crusts CD29-2 and D11-1 (Ling et al., 1997). The Cenozoic $^{187}Os/^{188}Os$ seawater curve is used for age determination (Peucker-Ehrenbrink & Ravizza, 2012). The region highlighted in yellow, from ~7 to 4.5 Ma shows deviation from regional seawater at Davidson Seamount. Error bars for ε_{Nd} and $^{206}Pb/^{204}Pb$ are 2 standard deviation. for all analyses of the USGS A-1 nodule standard, n = 16 and 85, respectively. Error for $^{187}Os/^{188}Os$ is 2 standard deviation of A-1 excluding the lowest three values, two of which had contaminations on ^{185}Re, n = 13. Instrumental error greater than the 2 standard deviation of A-1 is shown for individual points.

more radiogenic $^{206}Pb/^{204}Pb$ and lower $^{207}Pb/^{206}Pb$ values are observed between 5.5 and 4.8 ± 0.5 Ma (Figure 4; supporting information Figure S5 and Data Set S3). A more detailed view of the lead data can be found in the supporting information (Christensen, 1997; Nielsen et al., 2011) (supporting information Figure S5). In contrast, Pb isotope ratios in Fe-Mn crusts D173-R2 and D11-4 from Taney B and Hoss Seamounts do not show any significant changes during that period.

5. Discussion

5.1. Isotope Excursions in California Margin Fe-Mn Crusts

The deviation of $^{187}Os/^{188}Os$ from the Cenozoic Os isotope seawater curve toward more radiogenic values from at least 6.8 ± 0.5 to 4.5 ± 0.5 Ma is accompanied by Nd isotope deviations recorded in the two Davidson Seamount Fe-Mn crusts (which are closest to the MC) over a similar time period, which also overlaps with a brief excursion toward radiogenic Pb isotope values in one of the Davidson Seamount Fe-Mn crusts (T145-R9; Figure 5). The change toward more radiogenic Os isotope values relative to the $^{187}Os/^{188}Os$ isotope seawater curve in the four Fe-Mn crusts from Davidson and Taney Seamounts was surprising given the long residence time, in comparison to Nd and Pb, and largely uniform distribution of Os in the global ocean (Levasseur et al., 1999; Peucker-Ehrenbrink & Ravizza, 2000, 2012). Estimates of the residence time of osmium in seawater vary from few thousand to about 50 kyr, pegging this element at the transition between an ocean-wide well-mixed reservoir (Levasseur et al., 1999) and tracers that can show regional variations in isotope composition (Paquay & Ravizza, 2012). Having such a residence time not only makes the marine Os isotope system responsive to climatic (short-term) and tectonic (long-term) forcing, but it also increases the likelihood of observing strong regional forcing from inputs with isotope signatures very different from that of contemporaneous seawater. The few water column profiles of Os are generally consistent with conservative behavior in seawater with a modern seawater $^{187}Os/^{188}Os$ ~1.06, though indications of nonconservative behavior in oxygen minimum zones have been observed (Levasseur et al., 1999; Peucker-Ehrenbrink & Ravizza, 2000; Sharma & Wasserburg, 1997; Woodhouse et al., 1999; Zeng et al., 2014). Osmium is also not conservative in estuaries. The few systems that have been studied act as a sink for Os with 20% to 30% of Os removed from the dissolved phase as concentration of Os in the suspended phase increases with increasing salinity (Martin et al., 2001; Sharma et al., 2007). Approximately 80% of the Os in seawater is of continental crustal origin, with hydrothermal, and extraterrestrial sources accounting for the remainder (Sharma & Wasserburg, 1997; Williams & Turekian, 2002). Fresh Mid-Ocean Ridge Basalt (MORB) is characterized by a $^{187}Os/^{188}Os$ of 0.133 (Gannoun et al., 2006; Zeng et al., 2014), slightly more radiogenic than unaltered abyssal peridotite ($^{187}Os/^{188}Os$ = 0.121; Brandon et al., 2000; Harvey et al., 2011; Zeng et al., 2014). Hydrothermal fluids at the Juan de Fuca Ridge, approximately 1,200 km north of the MCS, have $^{187}Os/^{188}Os$ values that range from 0.11 to 1.04 (Sharma et al., 2000, 2007). Hydrothermal seafloor massive sulfides have $^{187}Os/^{188}Os$ ratios between 0.968 and 1.209 (Zeng et al., 2014). While hydrothermal input could provide a radiogenic source for $^{187}Os/^{188}Os$ it could not provide a radiogenic source for Nd, as Nd is scavenged within or directly adjacent to hydrothermal systems (van de Flierdt et al., 2004). Hydrothermal inputs are therefore unlikely to have provided the radiogenic Nd

observed in Davidson Seamount crusts or the radiogenic Os observed in Taney and Davidson Seamount Fe-Mn crusts over the same period.

Extraterrestrial sources have a much less radiogenic $^{187}Os/^{188}Os$ signature than seawater of ~0.12–0.13 and have high Os concentrations (Brandon et al., 2006; Horan et al., 2003; Peucker-Ehrenbrink & Ravizza, 2000). Extraterrestrial material would therefore cause an excursion in the opposite direction to that observed in Davidson and Taney Seamount Fe-Mn crusts. Fe-Mn crusts with $^{187}Os/^{188}Os$ that plot below the Os seawater curve have been shown to contain micrometeorite fragments (Klemm et al., 2005; Peucker-Ehrenbrink & Ravizza, 2000). A few individual Fe-Mn crust samples analyzed here, including a data point at ~2.7 Ma from Hoss Seamount D11-4, show less radiogenic values relative to the Os seawater curve and have high-count rates (indicating high Os concentration) that we attribute to the presence of extraterrestrial material.

Increased burial of Os caused by enhanced primary productivity or decrease in deep water dissolved oxygen concentrations also do not affect the $^{187}Os/^{188}Os$ values as evident from measurements at ODP Site 849 that is located in the eastern equatorial Pacific (Dalai et al., 2005).This shows that change in water column processes such as primary productivity may affect the concentrations of Os and possibly Nd and Pb available to be incorporated into Fe-Mn crusts, but are unlikely to impact the isotope ratios recorded in the crusts. Indeed, unlike Nd concentration data that mimic nutrient-like depth profiles in seawater, ε_{Nd} appears to trace water masses and does not covary with chlorophyll a (Hu et al., 2016; Jeandel & Oelkers, 2015; Stichel et al., 2012). Lead isotopes are even less likely to be influenced by primary productivity, as Pb is not utilized by primary producers (Chow & Patterson, 1962; Flegal & Patterson, 1983). Hence, changes in marine primary productivity cannot explain the isotope offsets observed prior to ~4.5 ± 0.5 Ma in the Fe-Mn crusts collected close to the MCS.

Terrestrial aeolian dust and fluvial inputs are other sources of Os that must be considered. Dust transported to seawater has a globally averaged $^{187}Os/^{188}Os$ of 1.05 ± 0.2 and an Os concentration of ~30 pg/g (Peucker-Ehrenbrink & Jahn, 2001), but little of the Os in dust is expected to dissolve in seawater. The $^{187}Os/^{188}Os$ of average fluvial inputs is likely more radiogenic (~1.4) than average crustal material because easily weathered Os-rich lithologies, such as sediments rich in organic matter, have more radiogenic isotope values (Dubin & Peucker-Ehrenbrink, 2015; Peucker-Ehrenbrink & Ravizza, 2000). Overall, aerosol deposition contributes only a small fraction of the overall continental Os input to the ocean (Sharma & Wasserburg, 1997; Williams & Turekian, 2002). Accordingly, this favors fluvial input of Os into the California margin through the MCS as the most likely source of radiogenic Os to the Davidson and Taney Seamounts. Inputs from rivers transporting dissolved and particulate terrestrial material have been shown to affect local seawater $^{187}Os/^{188}Os$ (Martin et al., 2000; Oxburgh et al., 2007; Sharma et al., 1999) and may explain the local deviation in the crusts when compared to the seawater $^{187}Os/^{188}Os$ curve.

Neodymium has a residence time in seawater of 400–950 years, shorter than the ~1,000 year mixing time of the global ocean (David et al., 2001; Lacan et al., 2012; Piepgras et al., 1979). The Nd isotope composition of seawater is controlled by the isotopic signature of the source inputs, which in turn are controlled by weathering of source rocks, which causes different water masses in the oceans and different ocean basins to have distinct Nd isotope values (Frank, 2002; Goldstein et al., 1984; van de Flierdt et al., 2016). In estuaries, Nd is rapidly (within ~3 weeks) released from suspended sediments (Rousseau et al., 2015). For example, in the Amazon estuary, the ε_{Nd} values were shown to change from a more radiogenic dissolved river end-member by about −1.8 ε_{Nd} units, toward less radiogenic values, as the dissolved Nd was coagulated by colloidal matter, to a less radiogenic value consistent with suspended fluvial material (Rousseau et al., 2015). This is consistent with models that suggest that sediment release from fluvial input is a significant source of Nd in seawater (Rousseau et al., 2015; van de Flierdt et al., 2016). Aeolian inputs may also be an important source of Nd to the ocean, but aeolian and fluvial inputs alone cannot account for the mass balance of Nd in seawater (Goldstein et al., 1984; van de Flierdt et al., 2016). Submarine groundwater discharge is another source of Nd that may influence seawater near the continental margin (Du et al., 2016; Jeandel & Oelkers, 2015; Lacan & Jeandel, 2005). Additional processes can redistribute Nd in seawater, including reversible scavenging, fluxes from sediment pore waters, and chemical reactions between terrestrial particles and seawater, collectively called "boundary exchange" (Abbott et al., 2015a, 2015b; Du et al., 2016; Jeandel & Oelkers, 2015; Lacan & Jeandel, 2005). The Nd isotope signature of Fe-Mn crusts is generally thought to reflect changes in water masses, but continental input, benthic flux, and boundary exchange processes within the continental shelf and slope must also be taken into account, particularly in coastal areas

(Abouchami et al., 1997; Jeandel & Oelkers, 2015; van de Flierdt et al., 2016). In Fe-Mn crusts, Nd does not re-equilibrate with modern seawater or diffuse noticeably within the crust, thus preserving the original water column signal over time (Abouchami et al., 1997; Bau & Koschinsky, 2006; Frank, 2002).

Model calculations using ε_{Nd} over the past 14 Myr from North Pacific Fe-Mn crusts indicate that dust dissolution provided just a few percent of dissolved Nd in this region for the time of interest, >6.8 to 4.5 Ma (Pettke et al., 2000; van de Flierdt et al., 2004). Rivers are the main source of sediment to the central California margin, a region where sediment input is often dominated by episodic floods (Best & Griggs, 1991; Edwards, 2002; Lewis et al., 2002). Fluvial sediment is normally transported past the littoral zone and may be deposited on or off the continental shelf (Edwards, 2002; Lewis et al., 2002). On-shelf sediments can subsequently be advected, or resuspended during high-energy events, and transported significant distances alongshore (Best & Griggs, 1991; Edwards, 2002; Ogston & Sternberg, 1999).

Resuspension and transport of sediment may affect the concentrations and isotope signatures of Os and Nd. Marine Os is scavenged in estuary and coastal zone sediments, reducing the flux of dissolved fluvial Os transported to the ocean (Martin et al., 2000, 2001; Williams & Turekian, 2004). However, it is also possible that changes in salinity may cause the release of previously nonsoluble Os sequestered in sediments (Martin et al., 2001). It has been well documented that the release of Nd from sediments along continental margins due to the dissolution of terrestrial particulate material can change the ε_{Nd} signature of regional seawater (Arsouze et al., 2007; Garcia-Solsona et al., 2014; Jeandel & Oelkers, 2015; Lacan & Jeandel, 2005; Stichel et al., 2012). Sediment resuspension and release of Nd and possibly Os are potential sources of these elements to California margin seawater from >6.8 to 4.5 $\pm$ 0.5 Ma.

Like Os and Nd, Pb is considered to be a closed system in Fe-Mn crusts (Abouchami et al., 1997; Chen et al., 2013; Henderson & Burton, 1999; Ling et al., 2005). Experiments to study the behavior of Pb in an estuary environment provided evidence that dissolved and particulate Pb does undergo isotope exchange on time scales of hours to days (Chen et al., 2016). In seawater, Pb has a relatively short residence time of 80–100 years (Flegal & Patterson, 1983). This is significantly shorter than the residence times of Os and Nd. Lead is therefore expected to be more susceptible to local inputs, presuming sources are isotopically distinct from local seawater. As Pb isotope values vary considerably both spatially and temporally in the ocean it is difficult to determine what the local seawater value would have been prior to the influence from the MC. However, the large excursion toward radiogenic values at around 5.3 Ma in Davidson Seamount crust T145-R9 is not related to regional Pb isotope signatures, as evidenced by the absence of this excursion in Taney D173-R2 and Hoss D11-4 Fe-Mn crusts. The main sources of Pb to the oceans are aeolian dust, hydrothermal fluids, and fluvial input (Frank, 2002). As Fe-Mn crust T145-R9 does not show evidence of hydrothermal inputs around 5.3 Ma and dust is unlikely to have a high enough Pb concentration to alter the local seawater Pb isotopic composition so significantly, we consider fluvial inputs of radiogenic terrestrial material as the most likely cause of the excursion.

Evidence for terrestrial input into the California margin is also recorded in Ocean Drilling Program (ODP) Leg 167 Sites 1018 (2,477 mbsl) and 1020 (3,038 mbsl), located off of the central and northern California coast (Hovan et al., 2000) (Figure 1). Site 1018 is located ~75 km west of the northern Monterey Bay and has very high sedimentation rates that average 100–400 m/Myr in the late Pleistocene (Hovan et al., 2000). Site 1020 was drilled on the east flank of Gorda Ridge and has sedimentation rates averaging over 100 m/Myr (Hovan et al., 2000). Sediments recovered at these sites include biogenic silica and carbonate but are dominated by terrestrial clays and silts that make up 70–80% of the bulk sediment (Hovan et al., 2000). It was proposed that terrestrial sediment preserved at Site 1020 originated from input near the Pioneer Canyon (Hovan et al., 2000). The water depths and distance to the coastline at these ODP sites are comparable those of the Fe-Mn crusts from Taney and Davidson Seamounts and support our interpretation that terrestrial inputs in this region was very high and could have affected seawater chemistry 225 km from the coastline. Other cores collected on ODP Leg 167 from the same region including Site 1021 show sparse diatom preservation with an increase of terrestrial material from the late Miocene (7 Ma) through the early Pliocene (2.6 Ma) (Lyle et al., 2000). At Site 1021, sediment accumulation rates increased from ~18 m/Myr in the late-middle and early-late Miocene to ~30 m/Myr at ~7.6 Ma even though diatom preservation decreased during this time, indicating an increase in deposition of terrigenous material (Barron et al., 2002; Lyle et al., 2000).

5.2. Source Areas of Fluvial Input

To examine potential sources of the terrestrial material responsible for the more radiogenic signatures in Davidson Seamount Fe-Mn crust T145-R9, $^{207}Pb/^{206}Pb$ was plotted against ε_{Nd} (Figure 6). Source regions were selected inland from the MCS to incorporate possible catchment regions, and extended from north of San Francisco Bay to the Mojave Desert in the south, and to the Colorado Plateau in the east (Beard & Johnson, 1997; Cousens, 1996; Farmer et al., 2002; Feuerbach et al., 1993; Heumann & Davies, 1997; Miller et al., 2000; Reid & Ramos, 1996; Schott et al., 2004; Wannamaker et al., 2000; Wolff et al., 2005). Data over the period of interest, (~7.5 to 4 Ma) from central Pacific Fe-Mn crusts, outside the influence of the MCS, are used to represent open-ocean seawater isotope values, and data from D11-4 at Hoss Seamount are plotted as a regional control (Chen et al., 2013; Ling et al., 1997, 2005). The Pb and Nd compositions from Davidson Seamount rock samples were also used as a comparison (Castillo et al., 2010). Using Pb isotope data from terrestrial source rocks to identify the source of the dissolved marine material has inherent uncertainties as the Pb isotope composition of labile Pb can differ from that of the bulk rock (Erel et al., 1994; Frank, 2002). Minerals hosting Pb have different time-integrated U-Pb and Th-Pb compositions and different susceptibilities to weathering, resulting in variations between the Pb isotope composition of source rocks, weathered residues and dissolved loads (Erel et al., 1994; Frank, 2002). For this reason, more weight should be placed on the possible Nd sources.

The Colorado Plateau is not a likely source as it has a more positive ε_{Nd} and higher $^{207}Pb/^{206}Pb$ than the excursion in Davidson Fe-Mn crust T145-R9 (Beard & Johnson, 1997; Wannamaker et al., 2000; Wolff et al., 2005). The most likely source of the dissolved terrestrial material seems to be erosion of the Big Pine Volcanic Field along the border of the southern Sierra Nevada and western Basin and Range (Figure 6). However, it is not possible to exclude the granitic Sierra Nevada or Long Valley Caldera from the central Sierras as potential source regions, due to overlap in the data. In addition, the Salinian block, on which the head of the MCS rests, was derived from the southern Sierra Nevada by strike-slip motion (Barbeau et al., 2005;

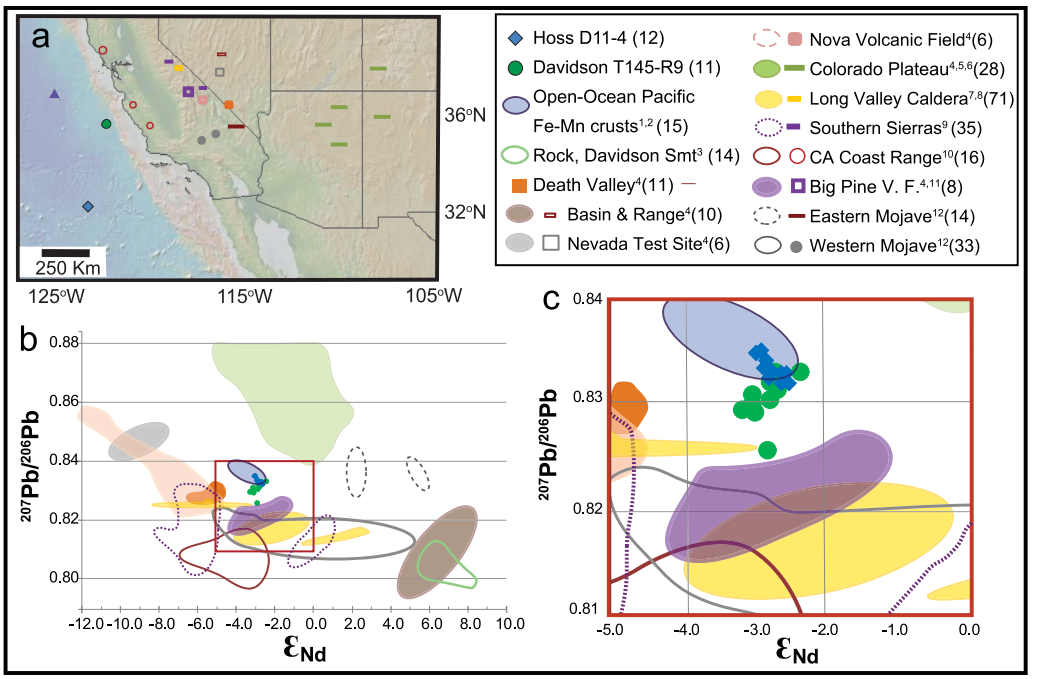

Figure 6. Source map for the south-western United States $^{207}Pb/^{206}Pb$ and $\varepsilon_{Nd;}$ (a) Location map of the south-western United States showing sample locations. (b) Plot of average $^{207}Pb/^{206}Pb$ and ε_{Nd} isotope values by region. (c) Inset box with individual $^{207}Pb/^{206}Pb$ and ε_{Nd} data points. Samples from Davidson and Hoss Fe-Mn crusts have 2–4 average Pb measurements for Nd each sample. Only data from 7 to 4.5 Ma is shown for California Margin and Central Pacific Fe-Mn crusts. All Nd data are normalized to JNdi-1 = 0.512115 for comparison. Southern Sierras includes data from Kern, San Joaquin, and Kings volcanic fields. References: 1. Ling et al. (1997); 2. Chen et al. (2013); 3. Castillo et al. (2010); 4. Beard and Johnson (1997); 5. Wannamaker et al. (2000); 6. Wolff et al. (2005); 7. Heumann and Davies (1997); 8. Cousens (1996); 9. Farmer et al. (2002); 10. Schott et al. (2004); 11. Reid and Ramos (1996); 12. Miller et al. (2000).

Chapman et al., 2014). Mixing of these source regions especially between Sierra Nevada sources that would mix in watersheds during transport westward into the San Joaquin Basin is quite likely. Additional mixing is likely between Sierra Nevada and Central Valley deposits.

While the input from the Sierra Nevada potentially explains the Pb and Nd data, an additional radiogenic source for Os is needed. Black shales of the Miocene Monterey Formation, underlie the southern section of the San Joaquin Basin, and sections along the California coastline including the Monterey Bay area (Anima et al., 2002) (Figure 1). Black shale as another potential source of radiogenic Os to the MCS could account for the deviation from the osmium isotope seawater curve toward more radiogenic $^{187}Os/^{188}Os$ prior to 4.5 ± 0.5 Ma. As radiogenic Os is efficiently mobilized during weathering of organic-rich shale and can lose 45–90% of its initial Os (Peucker-Ehrenbrink & Blum, 1998; Peucker-Ehrenbrink & Ravizza, 2000; Ravizza & Esser, 1993), such contributions can be even more radiogenic than average continental runoff ($^{187}Os/^{188}Os$ $\sim$1.4). Rivers draining shale deposits frequently have high $^{187}Os/^{188}Os$, and it has been proposed that black shale can provide a more radiogenic flux of Os than other rock types (Dalai & Ravizza, 2010; Ravizza & Esser, 1993; Singh et al., 1999). However, Os released from shale can be incorporated into secondary iron oxides and clay minerals during weathering and in rivers, which may restrict the flux of labile radiogenic Os (Dalai & Ravizza, 2010; Pierson-Wickmann et al., 2002). It is possible that a river or tributary sourced near the Big Pine Volcanic Field flowed through shale deposits in the San Joaquin Basin or near the coast resulting in a mixed particulate and dissolved load with an even more radiogenic $^{187}Os/^{188}Os$ signature flowing into the MC.

5.3. Timing the Incision of the Modern Monterey Canyon: Tectonic and Stratigraphic Evidence for Changes in Fluvial Input

As previously discussed, the isotope systems used in this study, Os, Nd, and Pb have very different residence times in seawater and in estuaries, and different behavior in the water column and in sediments. These factors are likely responsible for the differences in the records of the three isotope systems observed in the Fe-Mn crust samples studied. Out of the three elements studied Os has the longest residence time and most conservative behavior in seawater. It is therefore unsurprising that $^{187}Os/^{188}Os$ is the only isotope record reported here that shows deviations from ambient seawater isotope values at both the Davidson and Taney Seamounts, which we interpret as recording a strong local terrestrial input flux. Deviations of Nd and Pb isotope ratios from ambient seawater values are not observed in the Taney Seamount Chain, which is much farther from the coast. The less conservative behavior of these elements likely enables other processes to dissipate the terrigenous signal. Deviations from regional seawater $\varepsilon_{Nd,}$ and ^{204}Pb, ^{206}Pb, ^{207}Pb, ^{208}Pb, recorded in Hoss crust D11-4 are observed at Davidson Seamount but are of shorter duration than excursions in $^{187}Os/^{188}Os$ (Figure 5). The difference in sampling resolution may also be a contributing factor. Osmium was sampled at 2 mm intervals, while Nd was sampled at 0.3 mm intervals. Lead was sampled using a 50 μm wide laser spot at varying intervals (50 μm up to 1 mm) throughout the crust samples. Therefore, Os samples represent an average over a longer time interval whereas Pb data are averaged over a much shorter time interval. It is therefore not surprising that Os shows the least variation in between data points while Pb shows a large peak of short duration. Given the differences in residence time of these elements and the sampling resolution used, it is expected that the isotope records will be asynchronous even in response to the same forcing. The excursions toward radiogenic $^{206}Pb/^{204}Pb$ in crust T145-R9 from 5.8 to $\sim$4.9 Ma likely represent events in the delivery of terrestrial material on top of the already large dissolved and particulate loads affecting Nd and Os that were of sufficiently short duration to be averaged into the Nd and Os records.

$^{187}Os/^{188}Os$ records in the continent-proximal Fe-Mn crusts show that from some time before 6.8 ± 0.5 Ma and up to 4.5 ± 0.5 Ma the base of the MCS at Davidson Seamount was exposed to more radiogenic dissolved Os, compared with global/regional seawater. This radiogenic Os extended offshore and was also recorded in Fe-Mn crusts from the Taney Seamount chain. We propose that the radiogenic Os isotope signal reflects large volumes of terrestrial material transported into the system, a contention that is supported by the Nd and Pb isotope records from crusts on Davidson Seamount, located closer to shore. The timing of the radiogenic isotope excursions recorded in Fe-Mn crusts is consistent with an increase in right-lateral movement and increased canyon incision due to terrestrial input from 10 to 7 Ma, as proposed by Nagel et al. (1986) and Greene and Hicks (1990).

If it were possible to constrain plate motion in this region the incision rate of the MCS could be inferred based on canyon spacing. Unfortunately, constraining total right-lateral offset within Monterey Bay is challenging. The Salinian block and MCS are bisected by several faults including the San Gregorio Fault zone that caused northward strike-slip displacement of canyons in the Ascension Canyon System from the MCS (Greene & Hicks, 1990). In Monterey Bay, the San Gregorio Fault changes from the steep dip observed along the rest of the Fault to a moderate dip, indicating a change in the amount of strike-slip movement through Monterey Bay (Langenheim et al., 2013). This may be due to interaction between the San Gregorio Fault and other nearby faults or changes in fault geometry (Langenheim et al., 2013). This makes determining the slip rates for the San Gregorio Fault in Monterey Bay difficult, especially since reconstructions of slip rates and total offsets along the San Gregorio Fault vary widely (Dickinson et al., 2005; Langenheim et al., 2013). Therefore, it is not currently feasible to constrain the incision rate of the MCS and estimate the age of the modern MC using the spacing and depth of the canyons in the MCS.

Since the modern MC cuts through middle Miocene (15.97–11.63 Ma) strata, the exhumation of the canyon must have also postdated the middle Miocene (Greene, 1977; Greene & Hicks, 1990). This is supported by seismic-reflection profiles showing uninterrupted sedimentation in the canyons during the middle to late Miocene (15.97–5.33 Ma) with age data extrapolated to the offshore environment from nearshore cores (Greene, 1977; Greene & Hicks, 1990). Miocene (23.03–5.33 Ma) strata form uniformly thick flat beds on either side of the MC but thin toward the canyon center, indicating possible incision of the MC in the late Miocene to Pliocene (11.63–2.588 Ma) (Greene, 1977).

Around 10 Ma, the MC would have been located south and slightly inland of the canyon's present-day location and seaward from the paleo-coastline (DeMets & Merkouriev, 2016; Müller et al., 2008; Wilson et al., 2005) (Figure 1). This makes incision of the canyon system due to fluvial input around or before 10 Ma unlikely. However, submarine incision of the canyon due to down-canyon transport, hyperpycnal flows, and other turbidity currents is possible (Greene & Hicks, 1990; Mulder & Syvitski, 1995). Indeed, large volumes of terrestrial material were deposited into the San Joaquin Basin as evidenced by late Miocene and Pliocene (11.63–2.59 Ma) sedimentary deposits up to 2,470 m thick (Bowersox, 2004; Loomis, 1990). As the MC was located seaward from the paleo-coastline at 10 Ma, it is likely that exhumation of the canyon due to substantial fluvial input started after that time. However, by around 5 Ma the MC was on the paleo-coastline and would have been near the southern edge of the San Joaquin Basin coastline, hence we expect the increase in exhumation to have started sometime between 10 and 5 Ma. Based on our extrapolated Fe-Mn crust ages for sections with excursions from ambient seawater Os isotope values, we suggest that exhumation had started by $\sim$7 Ma. Around 7 Ma the head of the MC was near or above sea level and was located on the paleo-coastline, which is consistent with the $>6.8 \pm 0.5$ Ma onset of radiogenic Os and Nd isotope excursions in Davidson Seamount Fe-Mn crusts. Altogether, the tectonic, seismic and Fe-Mn crust age information indicate that incision of the MC commenced at some point after 10 Ma but before 7 Ma.

Until the end of the Miocene (5.33 Ma), the San Joaquin Basin southeast of the modern Monterey Bay was a shallow sea open to the Pacific on the western side and it captured westward drainage from the southern Sierra Nevada (Figure 2) (Bowersox, 2005; Loomis, 1988, 1990; Reid, 1995; Stanton & Dodd, 1997). Uplift of the South Coast Ranges starting at $\sim$5.4 Ma, closed the southern end of the basin, which was then connected to the Pacific only through the Priest Valley Strait that was likely $>$300 km north of the MC at $\sim$5 Ma (Bowersox, 2004, 2005; Loomis, 1990; Page et al., 1998). The Priest Valley Strait closed completely $\sim$2.3 Ma while the isotope excursion in Davidson and Taney Seamount Fe-Mn crusts had already started to approach open-ocean seawater values by $\sim$5.5 to 4.5 Ma (Bowersox, 2005). Therefore, draining of the San Joaquin Basin after it was cut off from open-ocean circulation could not have caused the isotope excursion.

The return to open-ocean seawater $^{187}Os/^{188}Os$ values in Davidson and Taney Seamount Fe-Mn crusts $\sim$4.5 Ma coincided with the Pliocene orogeny in western California (DeMets & Merkouriev, 2016; Page et al., 1998). Reconstruction of plate slip and rotation of the Sierra Nevada and Great Valley blocks with reference to the Pacific plate show that from 9 to 5.2 Ma the plates were parallel to the San Andreas Fault, but that from 5.2 Ma onward progressive clockwise rotation from the San Andreas Fault has occurred (DeMets & Merkouriev, 2016). The Sierra Nevada-Great Valley block and the Pacific plate began to converge at an angle orthogonal to the San Andreas Fault from 5.2 to 4.2 Ma (DeMets & Merkouriev, 2016). That coincided with the onset of the orogeny of the Santa Lucia Range starting around 6 Ma and estimated onset of shortening in central California at around 3.9 to 3.4 Ma (Ducea et al., 2003; Page et al., 1998). Most of Monterey Bay was

emergent by the late Pliocene to early Pleistocene (~3.6 to ~2.0 Ma) in part due to marine regression combined with regional uplift (Greene & Hicks, 1990; Nagel et al., 1986). We propose that uplift of the California Coast Range and emergence of the Monterey Bay region may have resulted in the termination of the isotope excursion by cutting off input from the San Joaquin Basin or by diverting riverine sources. This would have decreased the flux of continental runoff into the MC to such an extent that large-scale incision stopped and the continental isotope signature was diluted by mixing with regional seawater so the radiogenic continental isotope values were insufficient to affect the Fe-Mn crusts on Davidson and Taney Seamounts. A decrease in catchment basin area may also have decreased the amount of fluvial material transported into the MCS. In addition, the uplift of the Coast Range may have caused a change in the type of sediment transported from fine-grained material more susceptible to resuspension and more prone to dissolution, to a coarser-grained fluvial sediment load and a reduced dissolved flux. This also may have contributed to the change in Fe-Mn crust Os, Nd, and Pb isotope values toward compositions consistent with regional seawater at ~4.5 ± 0.5 Ma

Results presented here along with regional tectonic reconstructions help to constrain the start of modern MC exhumation to the late Miocene (11.63 to 6.8 ± 0.5 Ma) and termination of this event by ~4.5 Ma. This timing is earlier than the late Pliocene (~2.60 Ma) exhumation of the modern MC as proposed by Greene and Hicks (1990). There is also no evidence in the Os, Nd, or Pb isotope records from any of the Fe-Mn crusts for a second separate event occurring in the Pleistocene (<2.6 Ma) as proposed by Greene (1977). However, a shorter-duration reincision event in the MCS since ~4 Ma that did not change the seawater isotope signature locally over several hundred thousand years and was therefore not recorded in Fe-Mn crusts is possible as indicated by continuing transport in the canyon and associated incision.

6. Summary

We analyzed Os, Nd, and Pb isotopes in Fe-Mn crusts from three seamounts, Davidson proximal to the MCS, Taney offshore from the MCS, and Hoss, well removed from the MCS. Four Fe-Mn crust records from Davidson and Taney Seamounts deviated from the Cenozoic seawater $^{187}Os/^{188}Os$ curve toward more radiogenic values from >6.8 ± 0.5 to 4.5 ± 0.5 Ma. We attribute this to enhanced input of radiogenic material to the MCS that started in late Miocene time between ~10 and 7 Ma and ended about 4.5 ± 0.5 Ma, causing the $^{187}Os/^{188}Os$ in the Fe-Mn crusts to return to a seawater-dominated isotopic signature. This is supported by concurrent more radiogenic ε_{Nd} and Pb in Fe-Mn crusts from Davidson Seamount when compared to regional seawater isotope values of similar ages from >6.8 ± 0.5 to 4.5 ± 0.5 Ma. These data constrain the start of modern MC exhumation to between 10 and 6.8 ± 0.5 Ma and provides a minimum age of 6.8 ± 0.5 Ma for the MC.

The only reasonable source of radiogenic Os also capable of accounting for the trends observed in Nd and Pb is fluvial input of continental material with a radiogenic $^{187}Os/^{188}Os$ signature transported through the MCS. The most likely origin of this material is from near the border of the southern Sierra Nevada and southern edge of the western Basin and Range. The timing of the end of the Os isotope excursion at 4.5 ± 0.5 Ma is concurrent, within error, with the orogeny of the California Coast Range. This may have led to a change in the source material, sediment type, or drainage configuration, thereby reducing the radiogenic signature of the fluvial material, which, resulted in seawater near the MCS reverting to regional values subsequently recorded in the Fe-Mn crusts.

Acknowledgments
Supporting data including data sets and Python code for Pb processing are available in the supporting information of this publication. Funding was provided by the United States Geological Survey Pacific Coastal and Marine Science Center Marine Minerals Group, the University of California Santa Cruz Scholarship for Re-Entry Women in Science, and the UCSC Earth and Planetary Science Department Waters Award. We would like to thank the Monterey Bay Aquarium Research Institute (MBARI) for providing samples and the crew of the R.V. *Western Flyer* as well as the operators of the ROV *Doc Ricketts* for sample collection. We thank the Captain and crew of the R/V *Farnella* cruise F7–87-SC as well as David Clague and Jenny Paduan for their assistance with sample collection. We are also grateful to Tristan Horner, Jeremy Owens, and Gretchen Swarr (WHOI ICPMS Facility) at the Woods Hole Oceanographic Institution for their assistance with sample preparation and analyses. We would also like to thank G. Green, K. Suzuki, and an anonymous reviewer for their thoughtful reviews.

References

Abbott, A. N., Haley, B. A., & McManus, J. (2015a). Bottoms up: Sedimentary control of the deep North Pacific Ocean's ε_{Nd} signature. *Geochimica et Cosmochimica Acta*, *154*, 186–200. https://doi.org/10.1016/j.gca.2015.01.010

Abbott, A. N., Haley, B. A., McManus, J., & Reimers, C. E. (2015b). The sedimentary flux of dissolved rare earth elements to the ocean. *Geology*, *43*(11), 1035–1038. https://doi.org/10.1130/G37114.1

Abouchami, W., Goldstein, S. L., Gazer, S. J. G., Eisenhauer, A., & Mangini, A. (1997). Secular changes of lead and neodymium in central Pacific seawater recorded by a Fe-Mn crust. *Geochimica et Cosmochimica Acta*, *61*(18), 3957–3974.

Anima, R. J., Eittreim, S. L., Edwards, B. D., & Stevenson, A. J. (2002). Nearshore morphology and late Quaternary geologic framework of the northern Monterey Bay Marine Sanctuary, California. *Marine Geology*, *181*(1–3), 35–54. https://doi.org/10.1016/S0025-3227(01)00260-2

Arsouze, T., Dutay, J.-C., Lacan, F., & Jeandel, C. (2007). Modeling the neodymium isotopic composition with a global ocean circulation model. *Chemical Geology*, *239*(1–2), 165–177. https://doi.org/10.1016/j.chemgeo.2006.12.006

Barbeau, D. L., Ducea, M. N., Gehrels, G. E., Kidder, S., Wetmore, P. H., & Saleeby, J. B. (2005). U-Pb detrital-zircon geochronology of northern Salinian basement and cover rocks. *Geological Society of America Bulletin*, *117*(3–4), 466–481. https://doi.org/10.1130/B25496.1

Barron, J. A., Lyle, M., & Koizumi, I. (2002). Late Miocene and early Pliocene biosiliceous sedimentation along the California margin. *Revista Mexicana de Ciencias Geologicas*, *19*(3), 161–169.

Bau, M., & Koschinsky, A. (2006). Hafnium and neodymium isotopes in seawater and in ferromanganese crusts: The "element perspective. *Earth and Planetary Science Letters*, *241*(3–4), 952–961. https://doi.org/10.1016/j.epsl.2005.09.067

Beard, B. L., & Johnson, C. M. (1997). Hafnium isotope evidence for the origin of Cenozoic basaltic lavas from the southwestern United States. *Journal of Geophysical Research*, *102*(B9), 20149–20178. https://doi.org/10.1029/97JB01731

Best, T. C., & Griggs, G. B. (1991). A sediment budget for the Santacruz littoral cell, California. *Society for Sedimentary Geology Special Publication*, *46*, 35–50.

Bonatti, E., Kraemer, T., & Abdulla, H. A. N. (1972). Classification and genesis of submarine iron-manganese deposits. In D. R. Horn (Eds.), *Ferromanganese deposits on the ocean floor* (pp. 149–166). Washington, DC: National Science Foundation.

Bowersox, J. R. (2004). *Community structure, faunal distribution, and environmental forcing of the extinction of marine molluscs in the Pliocene San Joaquin Basin, Central California* (PhD dissertation). Tampa, FL: University of South Florida.

Bowersox, J. R. (2005). Reassessment of extinction patterns of Pliocene molluscs from California and environmental forcing of extinction in the San Joaquin Basin. *Palaeogeography, Palaeoclimatology, Palaeoecology*, *221*(1–2), 55–82. https://doi.org/10.1016/j.palaeo.2005.02.004

Brandon, A. D., Snow, J. E., Walker, R. J., Morgan, J. W., & Mock, T. D. (2000). 190Pt-186Os and 187Re-187Os systematics of abyssal peridotites. *Earth and Planetary Science Letters*, *177*(3–4), 319–335.

Brandon, A. D., Walker, R. J., & Puchtel, I. S. (2006). Platinum–osmium isotope evolution of the Earth's mantle: Constraints from chondrites and Os-rich alloys. *Geochimica et Cosmochimica Acta*, *70*(8), 2093–2103. https://doi.org/10.1016/j.gca.2006.01.005

Burton, K. W., Bourdon, B., Birck, J.-L., Allègre, C. J., & Hein, J. R. (1999). Osmium isotope variations in the oceans recorded by FeMn crusts. *Earth and Planetary Science Letters*, *171*(1), 185–197. https://doi.org/10.1016/S0012-821X(99)00139-9

Castillo, P. R., Clague, D. A., Davis, A. S., & Lonsdale, P. F. (2010). Petrogenesis of Davidson Seamount lavas and its implications for fossil spreading center and intraplate magmatism in the eastern Pacific: Davidson fossil spreading center lava petrogenesis. *Geochemistry, Geophysics, Geosystems*, *11*, Q02005. https://doi.org/10.1029/2009GC002992

Chapman, A. D., Ducea, M. N., Kidder, S., & Petrescu, L. (2014). Geochemical constraints on the petrogenesis of the Salinian arc, central California: Implications for the origin of intermediate magmas. *Lithos*, *200–201*, 126–141. https://doi.org/10.1016/j.lithos.2014.04.011

Chen, M., Boyle, E. A., Lee, J.-M., Nurhati, I., Zurbrick, C., Switzer, A. D., & Carrasco, G. (2016). Lead isotope exchange between dissolved and fluvial particulate matter: A laboratory study from the Johor River estuary. *Philosophical Transactions of the Royal Society A: Mathematical, Physical and Engineering Sciences*, *374*, 1–20. https://doi.org/10.1098/rsta.2016.0054

Chen, T.-Y., Ling, H.-F., Hu, R., Frank, M., & Jiang, S.-Y. (2013). Lead isotope provinciality of central North Pacific Deep Water over the Cenozoic. *Geochemistry, Geophysics, Geosystems*, *14*, 1523–1537. https://doi.org/10.1002/ggge.20114

Chow, T. J., & Patterson, C. C. (1962). The occurrence and significance of lead isotopes in pelagic sediments. *Geochimica et Cosmochimica Acta*, *26*(2), 263–308. https://doi.org/10.1016/0016-7037(62)90016-9

Christensen, J. N. (1997). Climate and ocean dynamics and the lead isotopic records in Pacific ferromanganese crusts. *Science*, *277*(5328), 913–918. https://doi.org/10.1126/science.277.5328.913

Clague, D. A., Paduan, J. B., Duncan, R. A., Huard, J. J., Davis, A. S., Castillo, P. R., . . . DeVogelaere, A. (2009). Five million years of compositionally diverse, episodic volcanism: Construction of Davidson Seamount atop an abandoned spreading center: Davidson Seamount ages and glass. *Geochemistry, Geophysics, Geosystems*, *10*, Q12009. https://doi.org/10.1029/2009GC002665

Conrad, T., Hein, J. R., Paytan, A., & Clague, D. A. (2017). Formation of Fe-Mn crusts within a continental margin environment. *Ore Geology Reviews*, *87*, 25–40. https://doi.org/10.1016/j.oregeorev.2016.09.010

Coumans, J. P., Stix, J., Clague, D. A., & Minarik, W. G. (2015). The magmatic architecture of Taney seamount-A, NE Pacific Ocean. *Journal of Petrology*, *56*(6), 1037–1067. https://doi.org/10.1093/petrology/egv027

Cousens, B. L. (1996). Magmatic evolution of Quaternary mafic magmas at Long Valley Caldera and the Devils Postpile, California: Effects of crustal contamination on lithospheric mantle-derived magmas. *Journal of Geophysical Research*, *101*(B12), 27673–27689. https://doi.org/10.1029/96JB02093

Covault, J. A., Normark, W. R., Romans, B. W., & Graham, S. A. (2007). Highstand fans in the California borderland: The overlooked deep-water depositional systems. *Geology*, *35*(9), 783–786. https://doi.org/10.1130/G23800A.1

Dalai, T. K., & Ravizza, G. (2010). Investigation of an early Pleistocene marine osmium isotope record from the eastern equatorial Pacific. *Geochimica et Cosmochimica Acta*, *74*(15), 4332–4345. https://doi.org/10.1016/j.gca.2010.04.062

Dalai, T. K., Suzuki, K., Minagawa, M., & Nozaki, Y. (2005). Variations in seawater osmium isotope composition since the last glacial maximum: A case study from the Japan Sea. *Chemical Geology*, *220*(3–4), 303–314. https://doi.org/10.1016/j.chemgeo.2005.04.012

David, K., Frank, M., O'nions, R. K., Belshaw, N. S., & Arden, J. W. (2001). The Hf isotope composition of global seawater and the evolution of Hf isotopes in the deep Pacific Ocean from Fe–Mn crusts. *Chemical Geology*, *178*(1–4), 23–42. https://doi.org/10.1016/S0009-2541(00)00427-7

Davis, A. S., Gray, L. B., Clague, D. A., & Hein, J. R. (2002). The Line Islands revisited: New 40Ar/39Ar geochronologic evidence for episodes of volcanism due to lithospheric extension: Line Islands revisited. *Geochemistry, Geophysics, Geosystems*, *3*(3). https://doi.org/10.1029/2001GC000190

DeMets, C., & Merkouriev, S. (2016). High-resolution reconstructions of Pacific–North America plate motion: 20 Ma to present. *Geophysical Journal International*, *207*(2), 741–773. https://doi.org/10.1093/gji/ggw305

Dickinson, W. R., Ducea, M., Rosenberg, L. I., Greene, H. G., Graham, S. A., Clark, J. C., . . . Brabb, E. E. (2005). Net dextral slip, Neogene San Gregorio–Hosgri fault zone, coastal California: Geologic evidence and tectonic implications, *Geological Society of America Special Paper*, *391*, 1–43. https://doi.org/10.1130/0-8137-2391-4.1

Du, J., Haley, B. A., & Mix, A. C. (2016). Neodymium isotopes in authigenic phases, bottom waters and detrital sediments in the Gulf of Alaska and their implications for paleo-circulation reconstruction. *Geochimica et Cosmochimica Acta*, *193*, 14–35. https://doi.org/10.1016/j.gca.2016.08.005

Dubin, A., & Peucker-Ehrenbrink, B. (2015). The importance of organic-rich shales to the geochemical cycles of rhenium and osmium. *Chemical Geology*, *403*, 111–120. https://doi.org/10.1016/j.chemgeo.2015.03.010

Ducea, M., House, M. A., & Kidder, S. (2003). Late Cenozoic denudation and uplift rates in the Santa Lucia Mountains, California. *Geology*, *31*(2), 139–142. https://doi.org/10.1130/0091-7613(2003)031<0139:LCDAUR>2.0.CO;2

Edwards, B. D. (2002). Variations in sediment texture on the northern Monterey Bay National Marine Sanctuary continental shelf. *Marine Geology*, *181*(1–3), 83–100. https://doi.org/10.1016/S0025-3227(01)00262-6

Eittreim, S. L., Anima, R. J., & Stevenson, A. J. (2002). Seafloor geology of the Monterey Bay area continental shelf. *Marine Geology*, *181*(1), 3–34.

Erel, Y., Harlavan, Y., & Blum, J. D. (1994). Lead isotope systematics of granitoid weathering. *Geochimica et Cosmochimica Acta*, *58*(23), 5299–5306. https://doi.org/10.1016/0016-7037(94)90313-1

Farmer, G. L., Glazner, A. F., & Manley, C. R. (2002). Did lithospheric delamination trigger late Cenozoic potassic volcanism in the southern Sierra Nevada, California. *Geological Society of America Bulletin*, *114*(6), 754–768. https://doi.org/10.1130/0016-7606(2002)114<0754:DLDTLC>2.0.CO;2

Feuerbach, D. L., Smith, E. I., Walker, J. D., & Tangeman, J. A. (1993). The role of the mantle during crustal extension: Constraints from geochemistry of volcanic rocks in the Lake Mead area, Nevada and Arizona. *Geological Society of America Bulletin*, *105*(12), 1561–1575.

Fildani, A., & Normark, W. R. (2004). Late Quaternary evolution of channel and lobe complexes of Monterey Fan. *Marine Geology*, *206*(1–4), 199–223. https://doi.org/10.1016/j.margeo.2004.03.001

Flegal, A. R., & Patterson, C. C. (1983). Vertical concentration profiles of lead in the Central Pacific at 15°N and 20°S. *Earth and Planetary Science Letters*, *64*(1), 19–32. https://doi.org/10.1016/0012-821X(83)90049-3

Foster, G. L., & Vance, D. (2006a). In situ Nd isotopic analysis of geological materials by laser ablation MC-ICP-MS. *Journal of Analytical Atomic Spectrometry*, *21*(3), 288–296. https://doi.org/10.1039/B513945G

Foster, G. L., & Vance, D. (2006b). Negligible glacial–interglacial variation in continental chemical weathering rates. *Nature*, *444*(7121), 918–921. https://doi.org/10.1038/nature05365

Frank, M. (2002). Radiogenic isotopes: Tracers of past ocean circulation and erosional input. *Reviews of Geophysics*, *40*(1), 1–1. https://doi.org/10.1029/2000RG000094

Gannoun, A., Burton, K. W., Vigier, N., Gíslason, S. R., Rogers, N., Mokadem, F., & Sigfússon, B. (2006). The influence of weathering process on riverine osmium isotopes in a basaltic terrain. *Earth and Planetary Science Letters*, *243*(3–4), 732–748. https://doi.org/10.1016/j.epsl.2006.01.024

Garcia-Solsona, E., Jeandel, C., Labatut, M., Lacan, F., Vance, D., Chavagnac, V., & Pradoux, C. (2014). Rare earth elements and Nd isotopes tracing water mass mixing and particle-seawater interactions in the SE Atlantic. *Geochimica et Cosmochimica Acta*, *125*, 351–372. https://doi.org/10.1016/j.gca.2013.10.009

Goldstein, S. L., O'nions, R. K., & Hamilton, P. J. (1984). A Sm-Nd isotopic study of atmospheric dusts and particulates from major river systems. *Earth and Planetary Science Letters*, *70*(2), 221–236. https://doi.org/10.1016/0012-821X(84)90007-4

Graham, S. A., Carroll, A. R., & Miller, G. E. (1988). Kern River formation as a recorder of uplift and glaciation of the Southern Sierra Nevada. In S. A. Graham (Ed.), *Studies of the geology of the San Joaquin Basin* (Vol. 60, pp. 319–331). Stanford, CA: Pacific Section, SEPM.

Greene, H. G. (1977). *Geology of the Monterey Bay region, California* (Open-File Rep. 77–718, USGS Numbered Series). Reston, VA: U.S. Geological Survey.

Greene, H. G., & Hicks, K. R. (1990). Ascension-Monterey Canyon system: History and development. In R. E. Garrison (Ed.), *Geology and tectonics of the central California coast region—San Francisco to Monterey* (pp. 229–250). College Station, CA: Pacific Section AAPG.

Greene, H. G., Maher, N. M., & Paull, C. K. (2002). Physiography of the Monterey Bay National Marine Sanctuary and implications about continental margin development. *Marine Geology*, *181*(1), 55–82.

Greene, H. G., Stubblefield, W. L., & Theberge, A. E. (1989). *Geology of the Monterey submarine canyon system and adjacent areas, offshore central California* (Open-File Rep. 89–221, USGS Numbered Series). Reston, VA: U.S. Geological Survey.

Griggs, G. B., & Hein, J. R. (1980). Sources, dispersal, and clay mineral composition of fine-grained sediment off central and northern California. *Journal of Geology*, *88*(5), 541–566.

Halbach, P., & Puteanus, D. (1984). The influence of the carbonate dissolution rate on the growth and composition of Co-rich ferromanganese crusts from Central Pacific seamount areas. *Earth and Planetary Science Letters*, *68*(1), 73–87. https://doi.org/10.1016/0012-821X(84)90141-9

Harvey, J., Dale, C. W., Gannoun, A., & Burton, K. W. (2011). Osmium mass balance in peridotite and the effects of mantle-derived sulphides on basalt petrogenesis. *Geochimica et Cosmochimica Acta*, *75*(19), 5574–5596. https://doi.org/10.1016/j.gca.2011.07.001

Hein, J. R., & Koschinsky, A. (2014). Deep-ocean ferromanganese crusts and nodules. In H. Holland & K. Turekian (Eds.), *Treatise on geochemistry* (2nd ed., pp. 273–291). Amsterdam, the Netherlands: Elsivier. https://doi.org/10.1016/B978-0-08-095975-7.09879-X

Hein, J. R., Reid, J. A., Conrad, T. A., Dunham, R. E., Clague, D. A., Schulz, M. S., & Davis, A. S. (2010). *Seamounts and ferromanganese crusts within and near the U.S. EEZ off California—Data for RV Farnella cruise F7–87-SC*. Reston, VA: U.S. Geological Survey.

Henderson, G. M., & Burton, K. W. (1999). Using (234U/238U) to assess diffusion rates of isotope tracers in ferromanganese crusts. *Earth and Planetary Science Letters*, *170*, 169–179. https://doi.org/10.1016/S0012-821X(99)00104-1

Heumann, A., & Davies, G. R. (1997). Isotopic and chemical evolution of the post-caldera rhyolitic system at Long Valley, California. *Journal of Petrology*, *38*(12), 1661–1678.

Horan, M. F., Walker, R. J., Morgan, J. W., Grossman, J. N., & Rubin, A. E. (2003). Highly siderophile elements in chondrites. *Chemical Geology*, *196*(1–4), 27–42. https://doi.org/10.1016/S0009-2541(02)00405-9

Hovan, S. A., Kish, S. W., & Renyck, H. J. (2000). Late Pleistocene record of terrigenous mineral deposition along the Northern California Margin (Sites 1018 and 1020). In M. Lyle, I. Koizumi, C. Richter, & R. C. Moore Jr. (Eds.), *Proceedings of Ocean Drilling Program Leg 167 Scientific Results* (pp. 341–376). College Station, TX: Ocean Drilling Program. https://doi.org/10.2973/odp.proc.sr.167.207.2000

Hu, R., Piotrowski, A. M., Bostock, H. C., Crowhurst, S., & Rennie, V. (2016). Variability of neodymium isotopes associated with planktonic foraminifera in the Pacific Ocean during the Holocene and Last Glacial Maximum. *Earth and Planetary Science Letters*, *447*, 130–138. https://doi.org/10.1016/j.epsl.2016.05.011

Huang, K.-F., Blusztajn, J., Oppo, D. W., Curry, W. B., & Peucker-Ehrenbrink, B. (2012). High-precision and accurate determinations of neodymium isotopic compositions at nanogram levels in natural materials by MC-ICP-MS. *Journal of Analytical Atomic Spectrometry*, *27*, 1560–1567. https://doi.org/10.1039/c2ja30123g

Jacobsen, S. B., & Wasserburg, G. J. (1980). Sm-Nd isotopic evolution of chondrites. *Earth and Planetary Science Letters*, *50*(1), 139–155. https://doi.org/10.1016/0012-821X(80)90125-9

Jeandel, C., & Oelkers, E. H. (2015). The influence of terrigenous particulate material dissolution on ocean chemistry and global element cycles. *Chemical Geology*, *395*, 50–66. https://doi.org/10.1016/j.chemgeo.2014.12.001

Johnson, C. L., & Graham, S. A. (2007). Middle tertiary stratigraphic sequences of the San Joaquin basin, California. In *Petroleum systems and geologic assessment of oil and gas in the San Joaquin basin province, California* (U.S. Geol. Surv. Prof. Pap. 1713, pp. 1–18). Reston, VA: U.S. Geological Survey.

Klemm, V., Frank, M., Levasseur, S., Halliday, A. N., & Hein, J. R. (2008). Seawater osmium isotope evidence for a middle Miocene flood basalt event in ferromanganese crust records. *Earth and Planetary Science Letters*, *273*(1–2), 175–183. https://doi.org/10.1016/j.epsl.2008.06.028

Klemm, V., Levasseur, S., Frank, M., Hein, J., & Halliday, A. (2005). Osmium isotope stratigraphy of a marine ferromanganese crust. *Earth and Planetary Science Letters*, *238*(1–2), 42–48. https://doi.org/10.1016/j.epsl.2005.07.016

Lacan, F., & Jeandel, C. (2005). Neodymium isotopes as a new tool for quantifying exchange fluxes at the continent–ocean interface. *Earth and Planetary Science Letters*, *232*(3–4), 245–257. https://doi.org/10.1016/j.epsl.2005.01.004

Lacan, F., Tachikawa, K., & Jeandel, C. (2012). Neodymium isotopic composition of the oceans: A compilation of seawater data. *Chemical Geology*, *300–301*, 177–184. https://doi.org/10.1016/j.chemgeo.2012.01.019

Langenheim, V. E., Jachens, R. C., Graymer, R. W., Colgan, J. P., Wentworth, C. M., & Stanley, R. G. (2013). Fault geometry and cumulative offsets in the central Coast Ranges, California: Evidence for northward increasing slip along the San Gregorio–San Simeon–Hosgri fault. *Lithosphere*, *5*(1), 29–48. https://doi.org/10.1130/L233.1

Levasseur, S., Birck, J.-L., & Allègre, C. J. (1999). The osmium riverine flux and the oceanic mass balance of osmium. *Earth and Planetary Science Letters*, *174*(1–2), 7–23. https://doi.org/10.1016/S0012-821X(99)00259-9

Lewis, R. C., Coale, K. H., Edwards, B. D., Marot, M., Douglas, J. N., & Burton, E. J. (2002). Accumulation rate and mixing of shelf sediments in the Monterey Bay National Marine Sanctuary. *Marine Geology*, *181*(1–3), 157–169. https://doi.org/10.1016/S0025-3227(01)00265-1

Ling, H. F., Burton, K. W., O'nions, R. K., Kamber, B. S., von Blanckenburg, F., Gibb, A. J., & Hein, J. R. (1997). Evolution of Nd and Pb isotopes in Central Pacific seawater from ferromanganese crusts. *Earth and Planetary Science Letters*, *146*(1–2), 1–12. https://doi.org/10.1016/S0012-821X(96)00224-5

Ling, H.-F., Jiang, S.-Y., Frank, M., Zhou, H.-Y., Zhou, F., Lu, Z.-L., . . . Ge, C.-D. (2005). Differing controls over the Cenozoic Pb and Nd isotope evolution of deepwater in the central North Pacific Ocean. *Earth and Planetary Science Letters*, *232*(3–4), 345–361. https://doi.org/10.1016/j.epsl.2004.12.009

Loomis, K. B. (1988). Paleoenvironmental and paleoclimatic interpretation of upper Miocene - Pliocene Lithofacies and Macrobiota of the Etchegoin Group, Jacalitos Canyon, San Joaquin Valley, California. In S. A. Graham (Ed.), *Studies of the geology of the San Joaquin basin* (Vol. 60, pp. 303–318). Stanford, CA: Pacific Section SEPM.

Loomis, K. B. (1990). Depositional environments and sedimentary history of the Etchegoin Group, West-Central San Joaquin Valley, California In *Structure, stratigraphy and hydrocarbon occurrences of the San Joaquin Basin, CA* (pp. 231–246). College Station, CA: Pacific Section AAPG.

Lyle, M., Koizumi, I., Delaney, M. L., & Barron, J. A. (2000). Sedimentary record of the California Current system, middle Miocene to Holocene: A synthesis of Leg 167 results. In M. Lyle, I. Koizumi, C. Richter, & R. C. Moore Jr. (Eds.), *Proceedings of Ocean Drilling Program leg 167 Scientific Results* (pp. 341–376). College Station, TX: Ocean Drilling Program. https://doi.org/10.2973/odp.proc.sr.167.238.2000

Martin, C. E., Peucker-Ehrenbrink, B., Brunskill, G. J., & Szymczak, R. (2000). Sources and sinks of unradiogenic osmium runoff from Papua New Guinea. *Earth and Planetary Science Letters*, *183*(1–2), 261–274. https://doi.org/10.1016/S0012-821X(00)00281-8

Martin, C. E., Peucker-Ehrenbrink, B., Brunskill, G., & Szymczak, R. (2001). Osmium isotope geochemistry of a tropical estuary. *Geochimica et Cosmochimica Acta*, *65*(19), 3193–3200. https://doi.org/10.1016/S0016-7037(01)00654-8

Meade, R. H. (1969). Errors in Using modern stream-load data to estimate natural rates of denudation. *Geological Society of America Bulletin*, *80*(7), 1265–1274. https://doi.org/10.1130/0016-7606(1969)80[1265:EIUMSD]2.0.CO;2

Miller, J. S., Glazner, A. F., Farmer, G. L., Suayah, I. B., & Keith, L. A. (2000). A Sr, Nd, and Pb isotopic study of mantle domains and crustal structure from Miocene volcanic rocks in the Mojave Desert, California. *Geological Society of America Bulletin*, *112*(8), 1264–1279.

Mulder, T., & Syvitski, J. P. M. (1995). Turbidity currents generated at river mouths during exceptional discharges to the world oceans. *Journal of Geology*, *103*, 285–299. https://doi.org/10.1086/629747

Müller, R. D., Sdrolias, M., Gaina, C., & Roest, W. R. (2008). Age, spreading rates, and spreading asymmetry of the world's ocean crust: Digital models of the world's ocean crust. *Geochemistry, Geophysics, Geosystems*, *9*, Q04006. https://doi.org/10.1029/2007GC001743

Nagel, D. K., Mullins, H. T., & Greene, H. G. (1986). Ascension submarine canyon, California—Evolution of a multi-head canyon system along a strike-slip continental margin. *Marine Geology*, *73*(3), 285–310. https://doi.org/10.1016/0025-3227(86)90019-8

Nielsen, S. G., Gannoun, A., Marnham, C., Burton, K. W., Halliday, A. N., & Hein, J. R. (2011). New age for ferromanganese crust 109D-C and implications for isotopic records of lead, neodymium, hafnium, and thallium in the Pliocene Indian Ocean. *Paleoceanography*, *26*(2), 1–13. https://doi.org/10.1029/2010PA002003

Nielsen, S. G., Mar-Gerrison, S., Gannoun, A., LaRowe, D., Klemm, V., Halliday, A. N., . . . Hein, J. R. (2009). Thallium isotope evidence for a permanent increase in marine organic carbon export in the early Eocene. *Earth and Planetary Science Letters*, *278*, 297–307. https://doi.org/10.1016/j.epsl.2008.12.010

Ogston, A. S., & Sternberg, R. W. (1999). Sediment-transport events on the northern California continental shelf. *Marine Geology*, *154*(1–4), 69–82. https://doi.org/10.1016/S0025-3227(98)00104-2

Oxburgh, R., Pierson-Wickmann, A.-C., Reisberg, L., & Hemming, S. (2007). Climate-correlated variations in seawater $^{187}Os/^{188}Os$ over the past 200,000 yr: Evidence from the Cariaco Basin, Venezuela. *Earth and Planetary Science Letters*, *263*(3–4), 246–258. https://doi.org/10.1016/j.epsl.2007.08.033

Page, B. M., Coleman, R. G., & Thompson, G. A. (1998). Overview: Late Cenozoic tectonics of the central and southern Coast Ranges of California. *Geological Society of America Bulletin*, *110*(7), 846–876. https://doi.org/10.1130/0016-7606(1998)110<0846:OLCTOT>2.3.CO;2

Paquay, F. S., & Ravizza, G. (2012). Heterogeneous seawater $^{187}Os/^{188}Os$ during the Late Pleistocene glaciations. *Earth and Planetary Science Letters*, *349–350*, 126–138. https://doi.org/10.1016/j.epsl.2012.06.051

Paull, C. K., Ussler, W., Greene, H. G., Keaten, R., Mitts, P., & Barry, J. (2003). Caught in the act: The 20 December 2001 gravity flow event in Monterey Canyon. *Geo-Marine Letters*, *22*(4), 227–232. https://doi.org/10.1007/s00367-003-0117-2

Pettke, T., Halliday, A. N., Hall, C. M., & Rea, D. K. (2000). Dust production and deposition in Asia and the north Pacific Ocean over the past 12 Myr. *Earth and Planetary Science Letters*, *178*(3–4), 397–413. https://doi.org/10.1016/S0012-821X(00)00083-2

Peucker-Ehrenbrink, B., & Blum, J. D. (1998). Re-Os isotope systematics and weathering of Precambrian crustal rocks: Implications for the marine osmium isotope record. *Geochimica et Cosmochimica Acta*, *62*(19–20), 3193–3203. https://doi.org/10.1016/S0016-7037(98)00227-0

Peucker-Ehrenbrink, B., & Jahn, B. (2001). Rhenium-osmium isotope systematics and platinum group element concentrations: Loess and the upper continental crust. *Geochemistry, Geophysics, Geosystems*, *2*(10), 1061. https://doi.org/10.1029/2001GC000172

Peucker-Ehrenbrink, B., & Ravizza, G. (2000). The marine osmium isotope record. *Terra Nova*, *12*(5), 205–219. https://doi.org/10.1046/j.1365-3121.2000.00295.x

Peucker-Ehrenbrink, B., & Ravizza, G. (2012). Chapter 8—Osmium isotope stratigraphy. In F. M. Gradstein, J. G. Ogg, M. D. Schmitz, & G. M. Ogg (Eds.), *The geologic time scale* (pp. 145–166). Elsevier: Oxford, UK. https://doi.org/10.1016/B978-0-444-59425-9.00008-1

Piepgras, D. J., Wasserburg, G. J., & Dasch, E. J. (1979). The isotopic composition of Nd in different ocean masses. *Earth and Planetary Science Letters*, *45*, 223–236.

Pierson-Wickmann, A.-C., Reisberg, L., & France-Lanord, C. (2002). Behavior of Re and Os during low-temperature alteration: Results from Himalayan soils and altered black shales. *Geochimica et Cosmochimica Acta*, *66*(9), 1539–1548. https://doi.org/10.1016/S0016-7037(01)00865-1

Pyenson, N. D., Irmis, R. B., Lipps, J. H., Barnes, L. G., Mitchell, E. D., & McLeod, S. A. (2009). Origin of a widespread marine bonebed deposited during the middle Miocene Climatic Optimum. *Geology*, *37*(6), 519–522. https://doi.org/10.1130/G25509A.1

Ravizza, G., & Esser, B. K. (1993). A possible link between the seawater osmium isotope record and weathering of ancient sedimentary organic matter. *Chemical Geology*, *107*(3), 255–258. https://doi.org/10.1016/0009-2541(93)90186-M

Reid, M. R., & Ramos, F. C. (1996). Chemical dynamics of enriched mantle in the southwestern United States: Thorium isotope evidence. *Earth and Planetary Science Letters*, *138*(1–4), 67–81.

Reid, S. A. (1995). Miocene and Pliocene depositional systems of the southern San Joaquin basin and formation of sandstone reservoirs in the Elk Hills area, California. In *Cenozoic Paleogeography of the Western United States—II* (pp. 131–150). Stanford, CA: Pacific Section, Society of Economic Paleontologists and Mineralogists.

Rehkämper, M., Frank, M., Hein, J. R., & Halliday, A. (2004). Cenozoic marine geochemistry of thallium deduced from isotopic studies of ferromanganese crusts and pelagic sediments. *Earth and Planetary Science Letters*, *219*, 77–91.

Rousseau, T. C. C., Sonke, J. E., Jerome, C., van Beek, P., Souhaut, M., Boaventura, G., . . . Jeandel, C. (2015). Rapid neodymium release to marine waters from lithogenic sediments in the Amazon estuary. *Nature Communications*, *6* (7592), 1–8. https://doi.org/ 10.1038/ncomms8592

Ryan, W. B. F., Carbotte, S. M., Coplan, J. O., O'hara, S., Melkonian, A., Arko, R., . . . Zemsky, R. (2009). Global multi-resolution topography synthesis. *Geochemistry, Geophysics, Geosystems*, *10*, Q03014. https://doi.org/10.1029/2008GC002332

Scher, H. D., & Delaney, L. M. (2010). Breaking the glass ceiling for high resolution Nd isotope records in early Cenozoic paleoceanography. *Chemical Geology*, *269*(3–4), 329–338. https://doi.org/10.1016/j.chemgeo.2009.10.007

Schott, R. C., Johnson, C. M., & O'neil, J. R. (2004). Late Cretaceous tectonic history of the Sierra-Salinia-Mojave arc as recorded in conglomerates of the Upper Cretaceous and Paleocene Gualala Formation, northern California: Cretaceous history of the Gualala basin. *Journal of Geophysical Research*, *109*, B02204. https://doi.org/10.1029/2003JB002845

Sen, I. S., & Peucker-Ehrenbrink, B. (2014). Determination of osmium concentrations and ^{187} Os/^{188} Os of crude oils and source rocks by coupling high-pressure, high-temperature digestion with sparging OsO_4 into a multicollector inductively coupled plasma mass spectrometer. *Analytical Chemistry*, *86*(6), 2982–2988. https://doi.org/10.1021/ac403413y

Sharma, M., Rosenberg, E. J., & Butterfield, D. A. (2007). Search for the proverbial mantle osmium sources to the oceans: Hydrothermal alteration of mid-ocean ridge basalt. *Geochimica et Cosmochimica Acta*, *71*(19), 4655–4667. https://doi.org/10.1016/j.gca.2007.06.062

Sharma, M., & Wasserburg, G. J. (1997). Osmium in the rivers. *Geochimica et Cosmochimica Acta*, *61*(24), 5411–5416. https://doi.org/10.1016/S0016-7037(97)00329-3

Sharma, M., Wasserburg, G. J., Hofmann, A. W., & Butterfield, D. A. (2000). Osmium isotopes in hydrothermal fluids from the Juan de Fuca Ridge. *Earth and Planetary Science Letters*, *179*(1), 139–152. https://doi.org/10.1016/S0012-821X(00)00099-6

Sharma, M., Wasserburg, G. J., Hofmann, A. W., & Chakrapani, G. J. (1999). Himalayan uplift and osmium isotopes in oceans and rivers. *Geochimica et Cosmochimica Acta*, *63*(23–24), 4005–4012. https://doi.org/10.1016/S0016-7037(99)00305-1

Singh, S. K., Trivedi, J. R., & Krishnaswami, S. (1999). Re-Os isotope systematics in black shales from the Lesser Himalaya: Their chronology and role in the ^{187}Os/^{188}Os evolution of seawater. *Geochimica et Cosmochimica Acta*, *63*(16), 2381–2392. https://doi.org/10.1016/S0016-7037(99)00201-X

Stanton, R. J., & Dodd, J. R. (1997). Lack of stasis in late Cenozoic marine faunas and communities, central California. *Lethaia*, *30*(3), 239–256. https://doi.org/10.1111/j.1502-3931.1997.tb00466.x

Stichel, T., Frank, M., Rickli, J., & Haley, B. A. (2012). The hafnium and neodymium isotope composition of seawater in the Atlantic sector of the Southern Ocean. *Earth and Planetary Science Letters*, *317–318*, 282–294. https://doi.org/10.1016/j.epsl.2011.11.025

Tanaka, T., Togashi, S., Kamioka, H., Amakawa, H., Kagami, H., Hamamoto, T., . . . Dragusnu, C. (2000). JNdi-1: A neodymium isotopic reference in consistency with LaJolla neodymium. *Chemical Geology*, *168*, 279–281.

van de Flierdt, T., Frank, M., Lee, D.-C., Halliday, A. N., Reynolds, B. C., & Hein, J. R. (2004). New constraints on the sources and behavior of neodymium and hafnium in seawater from Pacific Ocean ferromanganese crusts. *Geochimica et Cosmochimica Acta*, *68*(19), 3827–3843. https://doi.org/10.1016/j.gca.2004.03.009

van de Flierdt, T., Griffiths, A. M., Lambelet, M., Little, S. H., Stichel, T., & Wilson, D. J. (2016). Neodymium in the oceans: A global database, a regional comparison and implications for palaeoceanographic research. *Philosophical Transactions of the Royal Society A: Mathematical, Physical and Engineering Sciences*, *374*(2081), 20150293. https://doi.org/10.1098/rsta.2015.0293

Wakabayashi, J., & Sawyer, T. L. (2001). Stream incision, tectonics, uplift, and evolution of topography of the Sierra Nevada, California. *Journal of Geology*, *109*(5), 539–562.

Wannamaker, P. E., Hulen, J. B., & Heizler, M. T. (2000). Early Miocene lamproite from the Colorado Plateau tectonic province, Southeastern Utah, USA. *Journal of Volcanology and Geothermal Research*, *96*(3–4), 175–190. https://doi.org/10.1016/S0377-0273(99)00146-8

Williams, G. A., & Turekian, K. K. (2002). Atmospheric supply of osmium to the oceans. *Geochimica et Cosmochimica Acta*, *66*(21), 3789–3791. https://doi.org/10.1016/S0016-7037(02)00922-5

Williams, G. A., & Turekian, K. K. (2004). The glacial–interglacial variation of seawater osmium isotopes as recorded in Santa Barbara Basin. *Earth and Planetary Science Letters*, *228*(3–4), 379–389. https://doi.org/10.1016/j.epsl.2004.10.004

Wilson, D. S., McCrory, P. A., & Stanley, R. G. (2005). Implications of volcanism in coastal California for the Neogene deformation history of western North America. *Tectonics*, *24*, TC3008. https://doi.org/10.1029/2003TC001621

Wolff, J. A., Rowe, M. C., Teasdale, R., Gardner, J. N., Ramos, F. C., & Heikoop, C. E. (2005). Petrogenesis of pre-caldera Mafic Lavas, Jemez Mountains volcanic field (New Mexico, USA). *Journal of Petrology*, *46*(2), 407–439. https://doi.org/10.1093/petrology/egh082

Woodhouse, O. B., Ravizza, G., Kenison Falkner, K., Statham, P. J., & Peucker-Ehrenbrink, B. (1999). Osmium in seawater: Vertical profiles of concentration and isotopic composition in the eastern Pacific Ocean. *Earth and Planetary Science Letters*, *173*(3), 223–233. https://doi.org/10.1016/S0012-821X(99)00233-2

Zeng, Z., Chen, S., Selby, D., Yin, X., & Wang, X. (2014). Rhenium–osmium abundance and isotopic compositions of massive sulfides from modern deep-sea hydrothermal systems: Implications for vent associated ore forming processes. *Earth and Planetary Science Letters*, *396*, 223–234. https://doi.org/10.1016/j.epsl.2014.04.017